**JHT Final Report (August 2009 – July 2011):**
**Improving Predictability of the Atlantic Warm Pool in Ocean Model for Assistance to Operational Hurricane Forecast**

Chunzai Wang[1], Sang-Ki Lee[2], and Carlos Lozano[3]
[1] NOAA/AOML, Miami, FL 33149
[2] CIMAS/University of Miami, Miami, FL 33149
[3] NOAA/NCEP/EMC, Camp Springs, MD 20746

## 1. Summary

The rationale for the current project is the recent scientific finding that the Atlantic warm pool (AWP) — a large body of warm water comprised of the Gulf of Mexico, the Caribbean Sea, and the western tropical North Atlantic — may add a value to improving the simulation of Atlantic tropical cyclone (TC) in operational hurricane forecast models. In particular, recent studies using both observations and models have shown that a large AWP reduces the vertical wind shear and increases the convective available potential energy over the main development region for Atlantic hurricanes, and thus facilitates the formation and development of Atlantic TCs (Wang et al. 2006; Wang et al., 2008a, 2008b). Therefore, our ultimate goal is to improve the forecast of the formation and intensification of Atlantic hurricanes in NCEP/EMC operational model, by improving the simulations of the AWP in that model during the Atlantic hurricane season of June to November.

We showed through our research during the JHT year-1 that HYCOM has a tendency to produce a large cold bias of up to 2degC in the AWP region. Such tendency is mostly hidden in the forced simulations because the model SST is always damped toward the observations in the forced simulations. The cold AWP bias is revealed only when HYCOM is thermally coupled to the atmospheric mixed layer model (AML). This is because nonphysical thermal interaction, which may be caused by the ocean model bias in the forced HYCOM simulations, is not allowed in the thermally coupled HYCOM simulations.

However, further model studies during the JHT year-2 suggest that such bias emerges very slowly. Over the AWP region, it takes about 4 ~ 5 months to develop a –1degC SST bias. Therefore, the cold AWP SST bias should not cause a serious problem in the 5-day forecast of the NCEP/EMC operational models. Nevertheless, we show in this report that the 5-day forecast error of RTOFS is as large as 2degC and usually negative. In particular, the cold SST error is largest in the deep tropics between equator and 10N, and in the southern Caribbean Sea. We suspect that the 5-day forecast error of RTOFS originates from a combination of many different sources, including the Cooper and Haines scheme, GFS weather forecast error, initialization, and 2DVAR data assimilation. It is demonstrated here that the application of a simple bias correction scheme could substantially reduce the 5-day forecast error of the RTOFS in the deep tropics and Southern Caribbean Sea.

After completing these tasks on the AWP bias in HYCOM and AWP predictability in RTOFS, we revisited a more fundamental issue of the role of AWP on Atlantic hurricane activity. The 2010 Atlantic hurricane season was extremely active, partly due to the persistence of the very large AWP throughout the season. However, no hurricanes made landfall in the United States, raising a question of what dictated the hurricane track. We used observations from 1970-2010 (also extending back to 1950) and numerical model experiments to find that the AWP not only affects the formation and intensification of Atlantic TCs, but also plays an important

role in the hurricane track. An eastward expansion of the AWP shifts the hurricane genesis location eastward, decreasing the possibility for a hurricane to make landfall. A large AWP also induces barotropic stationary wave patterns that weaken the North Atlantic subtropical high and produce the eastward steering flow anomalies along the eastern seaboard of the United States. Due to these two mechanisms, hurricanes are steered toward the northeast without making landfall in the United States.

Currently, NOAA seasonal outlook for hurricanes only issues a range of expected number of tropical storms, hurricanes and major hurricanes. In order to minimize the vulnerability of the society from anomalous weather extremes and to adequately organize the social resources for hurricane preparedness, a much more detailed seasonal outlook of Atlantic hurricane activity, such as storm track and regional landfalling probability, is required. Hopefully, our new findings here on the AWP-hurricane track relationship is further explored to lay a foundation for an improved NOAA seasonal outlook for hurricanes in the future.

## 2. AWP SST bias in thermally coupled HYCOM

We have setup a low-resolution ($1^o \times 1^o$) HYCOM for the Atlantic domain between $20^o$S and $70^o$N using RTOFS-Atlantic as the basic platform. At this stage, we are mainly working with this low-resolution stand-alone HYCOM to facilitate implementation, testing and verification of various model schemes and codes. So far, we have (1) evaluated the surface flux bias in Global Forecast System (GFS), (2) successfully implemented and tested the atmospheric mixed layer model (AML) and the mixed layer heat budget diagnosis scheme into the HYCOM, (3) performed low-resolution HYCOM experiments using the GFS, NCEP1 and a bias-corrected surface flux datasets with and without coupling with the AML, and (4) performed heat budget analysis to diagnose potential sources of AWP bias in the low-resolution HYCOM simulations with and without coupling with the AML. Finally, we have (5) explored the time evolution of AWP bias in the thermally coupled HYCOM simulations to determine whether the AWP bias inherent in HYCOM bias can emerge for short-term forecasts (from 6-hour to 1-week).

Our major findings are that (1) the shortwave radiative heat flux of the GFS dataset may not be realistic and add too much heat (about 40W/m$^2$ yearlong) into the AWP, (2) the low-resolution HYCOM tends to create a large cold bias in the AWP region due to its inherent oceanic heat flux errors, (3) when HYCOM is thermally coupled to the AML, the AWP cold bias can emerge during short-term simulations (1-week). Based on these findings, we have concluded that the thermally coupled HYCOM (AML-HYCOM), in combination with the mixed layer heat budget diagnosis scheme, is an effective and practical tool to identify and improve the inherent errors in HYCOM. Once the HYCOM bias is minimized to a satisfactory level, the AML-HYCOM forced with bias-correct surface fluxes could be used for RTOFS-Atlantic simulations in order to allow physically more realistic thermal interactions at the air-sea interface, thus to minimize thermodynamic inconsistency at the air-sea interface for initializing the HWRF-HYCOM. A brief summary of our achievements is provided here.

### 2.1. *Evaluation of surface flux bias in Global Forecast System* (*GFS*)

Earlier studies have demonstrated that HYCOM may have some limitations in simulating the thermodynamics of the AWP and thus requires some modifications and optimizations of model schemes and codes (Lee et al. 2005, 2007). Among others, the largest model uncertainty originates from the surface heat flux bias, since the magnitude of surface net heat flux into the AWP varies by as much as 100 W/m$^2$ among various observational surface flux products and

model-based reanalysis products typically used in regional simulations (Enfield and Lee 2005, Lee et al. 2005). Therefore, since the operational RTOFS-Atlantic is driven by the 3-hour forecast Global Forecast System (GFS), our first task is to evaluate the air-sea flux variables from the 3-hour forecast GFS, which are available for only 2008 and 2009 in NOAA national operational model archive and distribution system (http://www.nomads.noaa.gov).

A preliminary analysis of the 2008-2009 GFS dataset suggests that the GFS surface net heat flux into the AWP is too large (Figure 2-1a). In comparison to the Coordinated Ocean Research Experiments version-2 (CORE2) surface flux product (Large and Yeager 2008), an observation-based bias-corrected surface flux product, the 3-hour forecast GFS adds up to 50 $W/m^2$ of extra heat flux into the AWP region yearlong. Further analysis suggests that the GFS surface heat flux bias largely comes from the shortwave radiative heat flux component (Figure 2-1b), whereas other surface heat flux components of GFS are consistent with those of bias-corrected surface flux product (Figure 2-1c). The short wave radiative heat flux bias is slightly improved in the 6 hour forecast GFS (Figure 2-1b).

### 2.2. *Implantation of atmospheric mixed layer model* (*AML*)

In ocean-only models, such as HYCOM, the model ocean is always forced by the prescribed atmospheric conditions. Thus, in a strict sense, ocean–only models are useful only over the regions where ocean is predominantly forced by the atmosphere. Typically, flux forms of atmospheric forcing, such as short and long wave radiative heat fluxes, precipitation rate and wind stress, are directly used to force the ocean model. For latent and sensible heat fluxes, however, bulk equations are typically used to compute them interactively using wind speed, air humidity and air temperature at 10m (or 2m) along with the model SST. The main reason for not using the observed turbulent heat flux is that any bias in surface heat flux or in ocean model leads to local accumulation or depletion of oceanic heat, resulting in an unrealistic simulation of the upper ocean heat content. Therefore, using bulk formula is equivalent to damping the model SST toward observation. The main point is that it is certainly improper to evaluate an ocean model's performance if the SST in that model is damped toward observation.

An effective way to allow an ocean-only model to have realistic heat and freshwater exchanges at the air-sea interface is to couple the ocean model with an atmospheric mixed layer model (AML) of Seager et al. (1995). The AML solves advection-diffusion equations for air temperature and humidity in the planetary boundary layer (PBL). The air temperature and humidity above the PBL and the wind vector in the PBL are needed and they can be provided from, in the case of RTOF-Atlantic, the Global Forecast System (GFS). The benefit of coupling the AML to RTOFS-Atlantic is to allow physically more realistic thermal interactions at the air-sea interface, thus to minimize thermodynamic inconsistency at the air-sea interface for HWRF-HYCOM. We have successfully implemented and tested the AML model of Seager et al. (1995) in the low-resolution HYCOM.

### 2.3. *Low-resolution HYCOM experiments with and without thermal coupling*

In order to force the low-resolution HYCOM with the GFS air-sea flux, we need a longer time series air-sea flux dataset. Therefore, we construct a pseudo-GFS dataset for 1949-2009 periods by combining the 6-hour forecast of GFS for 2008-2009 and NCEP reanalysis-1 (NCEP1) for 1949-2009. First, for each air-sea flux variable, we compute the difference between GFS and NCEP1 in 2008-2009. For each air-sea flux variable, the difference in each month of 2008-2009 is added to the NCEP1 for the entire period of 1949-2009 to construct a pseudo-GFS

dataset. The main assumption here is that the difference in each air-sea flux variable between the GFS and NCEP1 in 2008-2009 repeats in all other years. Note that the GFS air-sea fluxes in 2008 and 2009 are not modified. Along with the pseudo-GFS and NCEP1, we construct a bias-corrected NCEP1 dataset for 1949-2009 periods by combining the CORE2 for 1971-2000 and NCEP1 for 1949-2009. In this case, for each air-sea flux variable, the NCEP1 climatology for 1971-2000 is simply replaced with the CORE2 climatology for 1971-2000 then the NCEP1 air-sea flux anomaly is added to the CORE2 climatology. The low-resolution HYCOM is forced with the three air-sea flux datasets, namely pseudo-GFS, NCEP1 and bias-corrected NCEP1 for 1949-2009 periods with and without thermal coupling to AML.

Figure 2-2 shows the observed and HYCOM-simulated AWP SST during June-July-August (JJA) and September-October-November (SON) in 2009. The black solid line represents 27.5$^{o}$C isotherm in 2008 to be compared with the colored AWP region of 2009. It is clear from this figure that the simulated AWP in the case of HYCOM_GFS is too warm especially in the Gulf of Mexico during JJA suggesting that the GFS surface heat flux adds too much heat into the AWP formation region (This issue is further investigated later in this section). On the other hand, when the low-resolution HYCOM is forced with the bias-corrected NCEP1, the simulated AWP is too small (or too cold). If we treat the bias-corrected NCEP1 surface flux dataset as the truth, what this means is that the oceanic processes in the low-resolution HYCOM, such as vertical turbulent mixing and advection, tend to create a large cold bias in the AWP region. A common feature in all simulations is that the coastal upwelling region near the northern coasts of Columbia and Venezuela is too cold, suggesting that large-scale eddy mixing is not large enough in the model simulations to dissipate the cold upwelled water in the region.

Figure 2-3 is identical to Figure 2-2, except that the simulated AWP SSTs are derived from the thermally coupled HYCOM (AML-HYCOM) during JJA and SON in 2009. The black solid line represents 27.5$^{o}$C isotherm in 2008 to be compared with the colored AWP region of 2009. The simulated AWP in the case of AML_HYCOM_GFS is slightly colder than observations. This is quite surprising because the 6-hour forecast GFS put excessive heat into the AWP region due to its shortwave radiative heat flux bias as shown in Figure 2-1. When the low-resolution HYCOM is forced with the bias-corrected NCEP1, the simulated AWP is almost gone. As pointed out earlier, what this means is that the oceanic processes in the low-resolution HYCOM tend to create a large cold bias in the AWP region. The cold bias is much more intensified when the HYCOM is thermally coupled to AML in comparison to the forced HYCOM simulations. This means that the AML-HYCOM provides a much stringent test for the performance of HYCOM.

### 2.4. *Mixed Layer Heat budget analysis in the AWP region*

Figure 2-4 shows the HYCOM-simulated mixed layer heat budget (upper 40m) for 2008-2009 averaged in the AWP region (100$^{o}$W-40$^{o}$W; 5$^{o}$N-30$^{o}$N). The heat budget terms include vertical mixing at 40m (VTRMIX), vertical advection at 40m (VRTADV) surface net heat flux (SURFLX), heat storage rate (STORAG), numerical vertical mixing (HYBMIX), horizontal diffusion (HRZDIF), and horizontal advection (HRZADV). See Lee et al. (2007) for the heat budget equation. This figure clearly shows that the surface net heat flux is the main driving force for the onset and decay of the AWP whereas the oceanic mixing and advection terms play a secondary role and tend to cool down the AWP in boreal summer and fall months (Lee et al. 2007). Consistent with Figure 2-1 and 2-2, the surface net heat flux in HYCOM_GFS is larger than the other two cases. Figure 2-5 is the same as Figure 2-4 except that the simulated AWP

heat budgets are derived from the thermally coupled HYCOM (AML-HYCOM) simulations. The overall heat budgets in the thermally coupled HYCOM simulations are similar to those of the forced HYCOM simulations.

Figure 2-6 shows the 2008-2009 surface flux components from two low-resolution HYCOM experiments, two AML-HYCOM experiments, and from two surface flux datasets (i.e., pseudo-GFS, and bias-corrected NCEP1). Note that the surface latent and sensible heat fluxes in the forced HYCOM simulations are recalculated by using the model simulated SST and bulk formulas. Similarly, the surface latent and sensible heat fluxes in the thermally coupled HYCOM simulations are recalculated by the model simulated SST and the AML model of Seager et al. (1995). Thus, the simulated heat flux is different from the original surface heat flux dataset used to force the HYCOM and AML-HYCOM. The latent heat flux in the original GFS dataset shows a reasonable range of values when it is compared with the bias-corrected NCEP1 dataset (Figure 2-6c). However, as pointed out in section 21, it is clear that the original GFS dataset adds up to 40 $W/m^2$ of extra shortwave radiative heat flux into the AWP region in comparison to the bias-corrected NCEP1 dataset (Figure 2-6b).

It is important to note that the simulated net surface flux into the AWP formation region is always too large in comparison to the bias-corrected NCEP1 net surface flux as shown in Figure 2-6a. This is largely due to the much-reduced surface latent cooling in the model simulations (Figure 2-6c) associated with the HYCOM's tendency to produces a large cold bias in the AWP formation region.

2.5. *Simulation of anomalous AWP SSTs in HYCOM with and without thermal coupling*

Figure 2-7 shows the anomalous AWP SST in June-November (JJASON) for the period of 1949-2009 simulated by HYCOM with and without thermal coupling to the AML. In the case of the forced HYCOM simulation, the correlation between the simulated and observed AWP SST anomaly is 0.79, which is larger than the case of the thermally coupled HYCOM (0.65~ 0.66). It is not surprising that the forced HYCOM simulation is better correlated with the observation than the thermally coupled HYCOM simulation because the AWP SST anomaly is basically relaxed to the observation in the forced HYCOM simulation. It is clear that the AML-HYCOM provides a much stringent test for the performance of HYCOM in capturing the AWP SST anomaly.

In order to better understand the regional pattern of model errors, the observed AWP SST anomaly in JJASON is regressed on to the observed and simulated SST anomalies in JJASON, as shown in Figure 2-8. As shown in Figure 2-8a, when the AWP is warm, the entire zonal strip of 10N-20N is warmed simultaneously. In the case of forced HYCOM simulations, the warming is largely located in the central tropical North Atlantic west of around 70W. The anomalous warming in the Caribbean Sea and off the West Africa is not well captured in the forced HYCOM simulation. In the case of thermally coupled simulations, in addition to the same problem, the warm SST anomaly is shifted southward around 10N. This means that the HYCOM has a tendency to generate a spatially inhomogeneous SST error pattern during anomalously warm and cold AWP events. Again, the AML-HYCOM truly reveals the inherent bias in the HYCOM, and thus provides a much stringent test for the performance of HYCOM in capturing the AWP SST anomaly.

2.6. *Time evolution of AWP SST bias in thermally coupled HYCOM*

We have shown here that HYCOM has a tendency to produce a large cold bias in the AWP region. Such tendency is mostly hidden in the forced simulations because the model SST is

damped toward the observations in the forced simulations. The cold AWP bias is revealed only when HYCOM is thermally coupled to the AML. This is because nonphysical thermal interaction, which may be caused by the ocean model bias in the forced HYCOM simulations, is not allowed the thermally coupled HYCOM simulations.

An important question is how fast the cold bias emerges. For instance, if it takes several years to develop, it is not a critical problem for short-term forecasts (from 6-hour to 1-week) in the NCEP/EMC's operational models (RTOFS-Atlantic and HWRF-HYCOM). Therefore, we have performed three additional experiments. First, HYCOM is forced with the three surface flux products of pseudo-GFS, NCEP1 and bias-corrected NCEP1 for the period of 1949-2007. Then, the thermal coupling is initiated in HYCOM from Jan/2007 and continued until Dec/2009. Shown in Figure 2-9 is the time evolution of simulated AWP SST errors for 2007-2009. The upper panel shows the AWP SST difference between the AML-HYCOM simulation and observation (HADISST). The lower panel shows the AWP SST difference between the AML-HYCOM and forced HYCOM simulations. The AWP SST bias develops quite fast. It takes about only 5 months for 1degC of cold bias to develop. This amounts to about 0.1degC of cold bias within 14days. Thus, it may not be negligible in short-term forecasts. It is also interesting to note that the AWP SST bias has a seasonal dependency, with a larger bias in boreal summer and fall and smaller bias in boreal winter and spring.

Figure 2-10 shows the expected spatial pattern of the SST bias growth within 15days in the thermally coupled HYCOM simulations. Focusing on the AML-HYCOM forced by the bias-corrected NCEP1, the entire mid-latitude North Atlantic between 20N-40N has a large cold bias. The cold bas is extended to the Gulf of Mexico. Interestingly, the Columbia basin is characterized with a relatively large warm bias. A further study is required to understand the spatial pattern of the SST bias growth.

### 2.7. *Recommendations*

Based on our researches during the JHT year-1 (August 1, 2009 - July 31, 2010), as summarized in this report, we provide the following two recommendations for the NCEP/EMC operational ocean model (RTOFS-Atlantic).

Suggestion-1). The 3-hour forecast GFS, which is used to force the RTOFS-Atlantic, has a large shortwave radiative heat flux bias in the AWP formation region. Therefore, *a bias correction of the GFS shortwave radiation is suggested*. This can be achieved by first constructing a pseudo-GFS climatology for 1971-2000 period then computing the difference between the pseudo-GFS climatology and the bias-corrected surface heat flux climatology of CORE2 following the methodology described in section 2.3. This difference is the bias-correction term to be added to the GFS shortwave radiative heat flux forecast. It is also suggested here that the 6-hour forecast GFS is used instead of the 3-hour forecast to reduce the shortwave radiative heat flux bias.

Suggestion-2). *It is recommended that the thermally coupled HYCOM (AML-HYCOM) with bias-corrected surface fluxes be implemented into RTOFS-Atlantic*. The thermally coupled RTOFS-Atlantic, in combination with the mixed layer heat budget diagnosis scheme, will provide an effective and practical tool to identify and improve the inherent errors in RTOFS-Atlantic. Ultimately, it will allow physically realistic thermal interactions at the air-sea interface, thus to minimize thermodynamic inconsistency at the air-sea interface for initializing the HWRF-HYCOM. However, it should be used as a diagnostic tool initially.

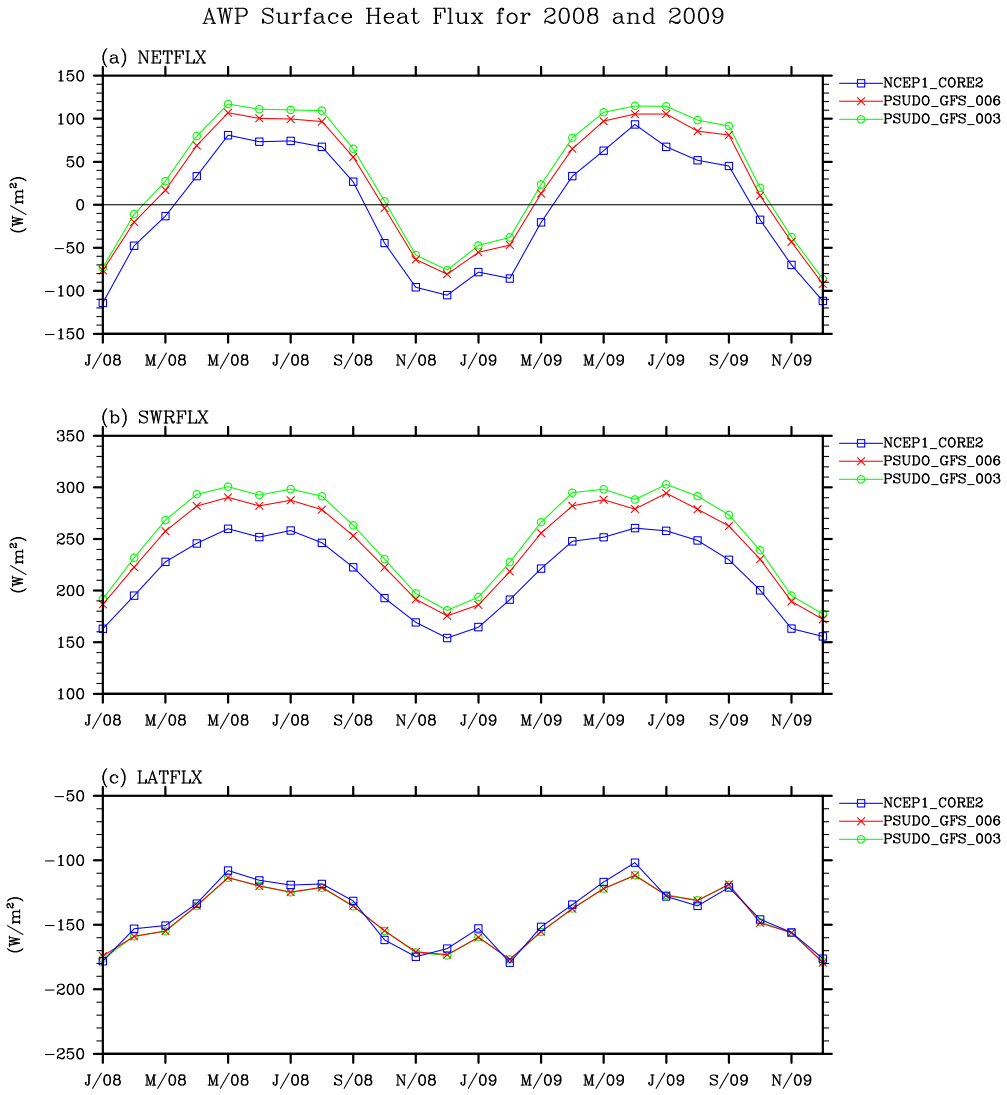


Figure 2-1. (a) Net surface heat flux, (b) shortwave heat flux, and (c) latent heat flux into the AWP formation region (100°W-40°W; 5°N-30°N) derived from the bias-corrected NCEP1, and 3-hour and 6-hour forecast of GFS for 2008-2009 period. Unit is W/m$^2$.

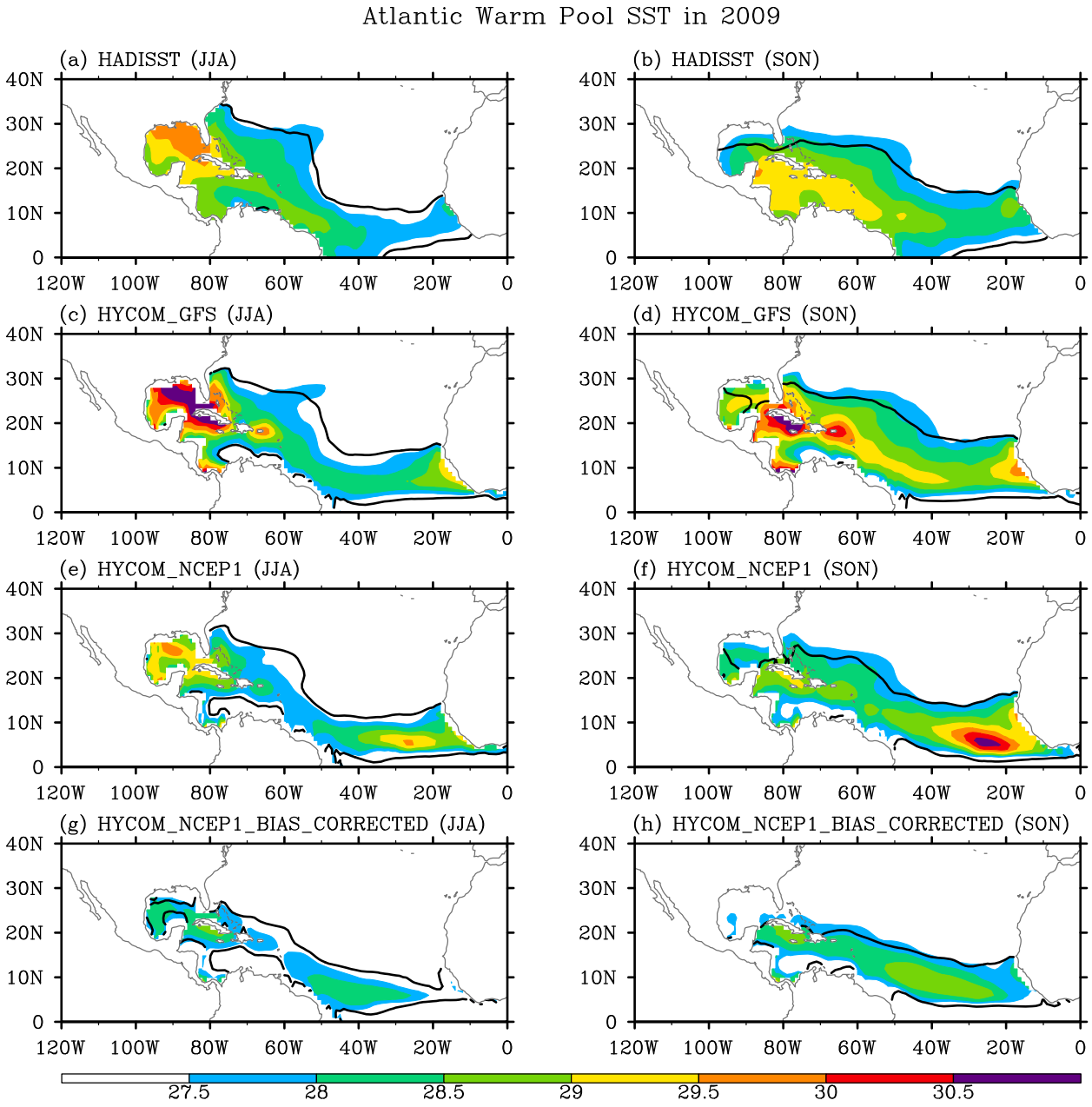


Figure 2-2. Observed and HYCOM-simulated AWP SST during June-July-August (JJA) and September-October-November (SON) in 2009. The black solid lines represent 27.5°C isotherm in 2008 to be compared with the colored AWP region of 2009. Unit is degC.

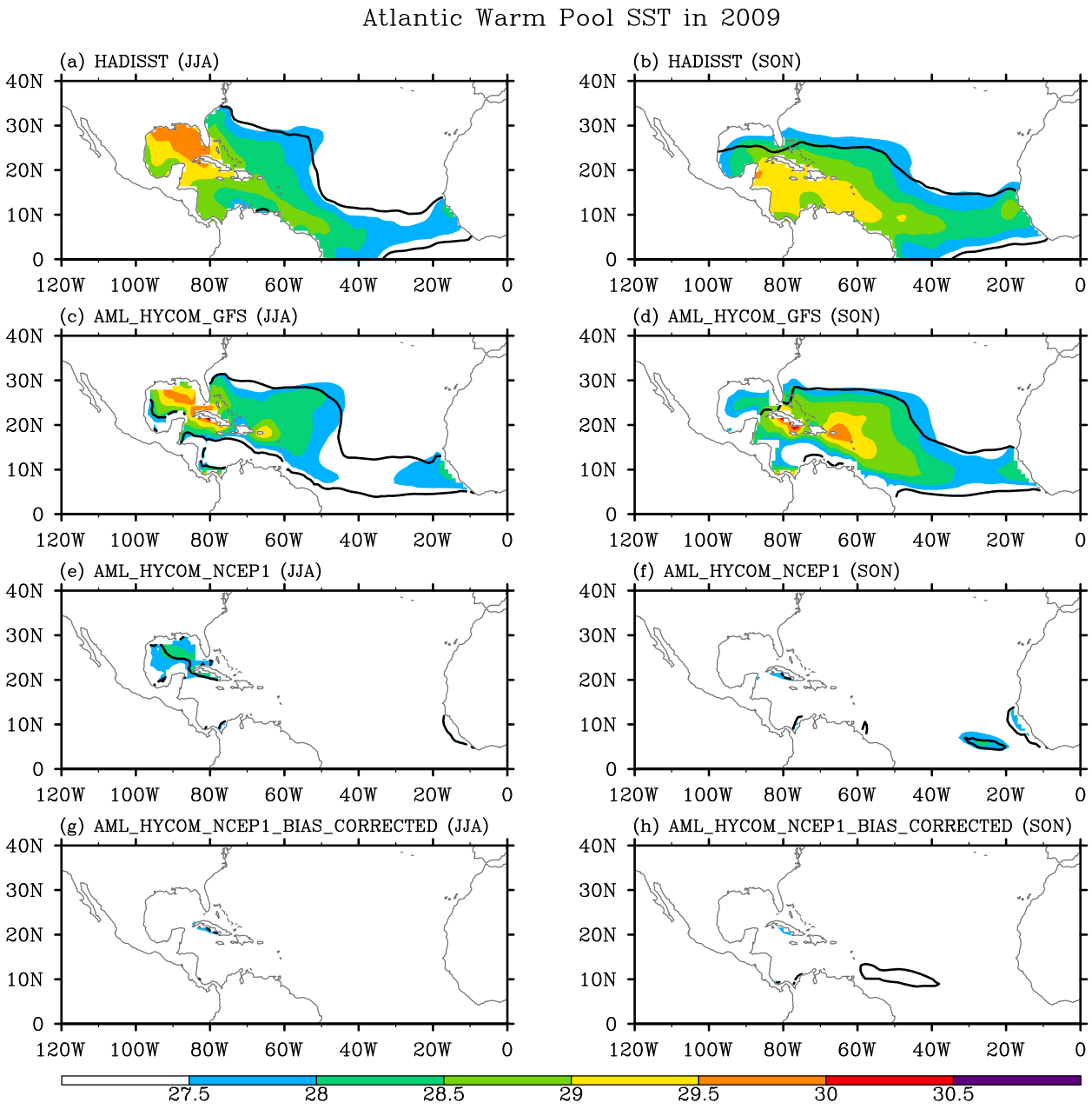


Figure 2-3. Observed and AML-HYCOM-simulated AWP SST during June-July-August (JJA) and September-October-November (SON) in 2009. The black solid lines represent 27.5°C isotherm in 2008 to be compared with the colored AWP region of 2009. Unit is degC.

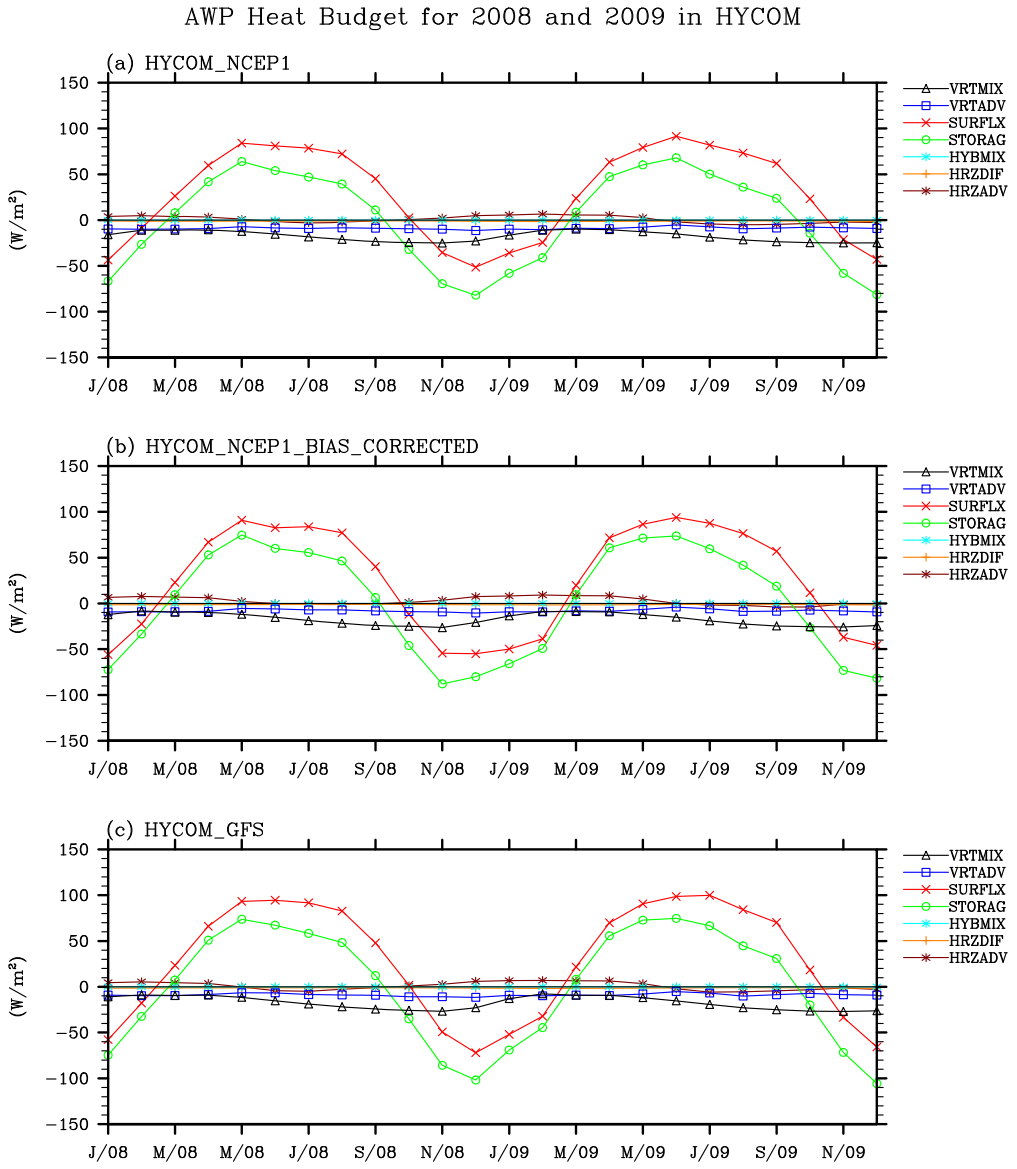


Figure 2-4. HYCOM-simulated mixed layer heat budget (upper 40m) for 2008-2009 averaged in the AWP region (100°W-40°W; 5°N-30°N). The heat budget terms include vertical mixing at 40m (vrtmix), vertical advection at 40m (vrtadv) surface net heat flux (surflx), heat storage rate (storag), numerical vertical mixing (hybmix), horizontal diffusion (hrzdif), and horizontal advection (hrzadv). See Lee et al. (2007) for the head budget equation. Unit is W/m$^2$.

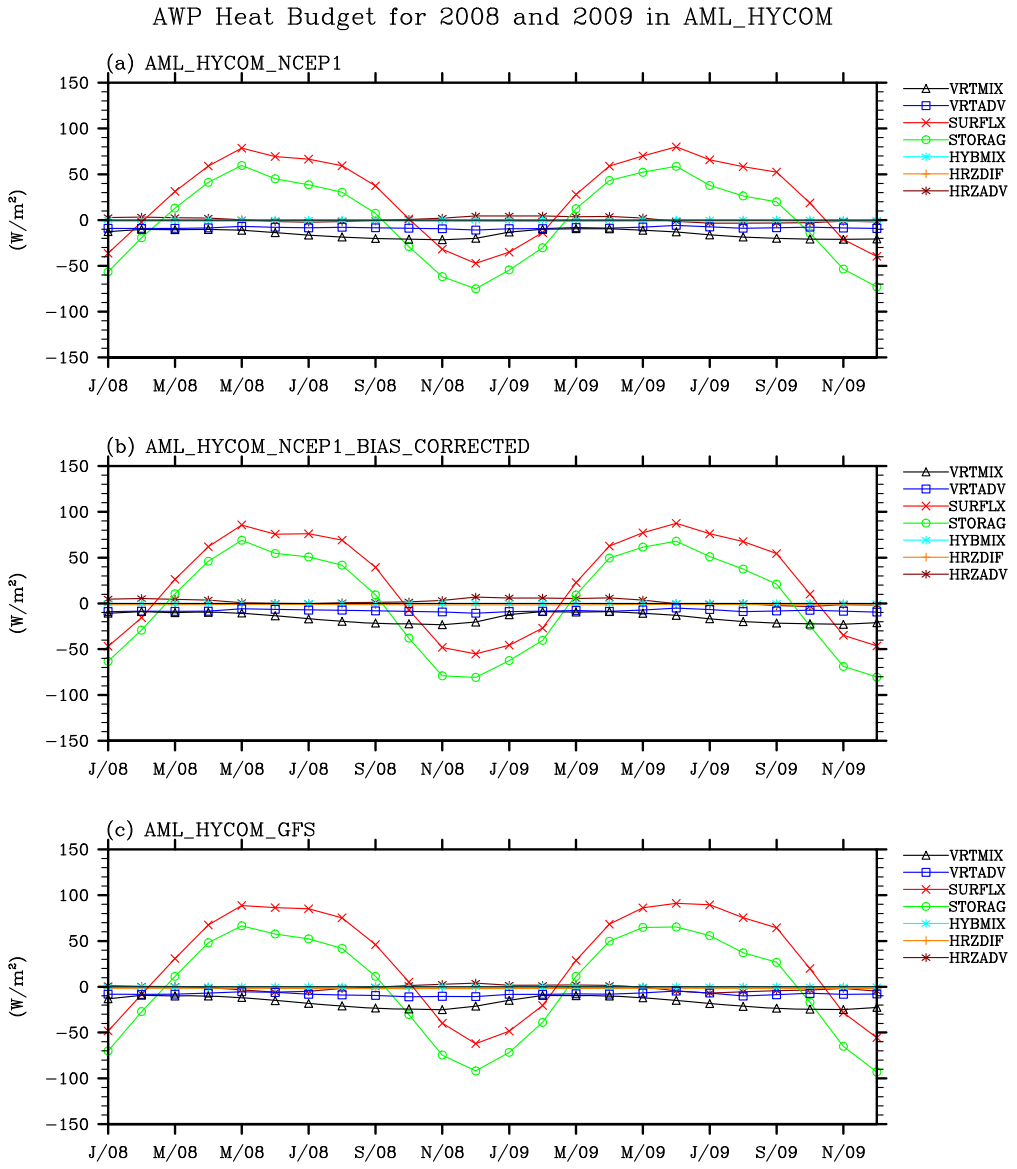


Figure 2-5. This is same as Figure 2-4 except that the simulated AWP heat budgets are derived from the thermally coupled HYCOM (AML-HYCOM) simulations. Unit is W/m$^2$.

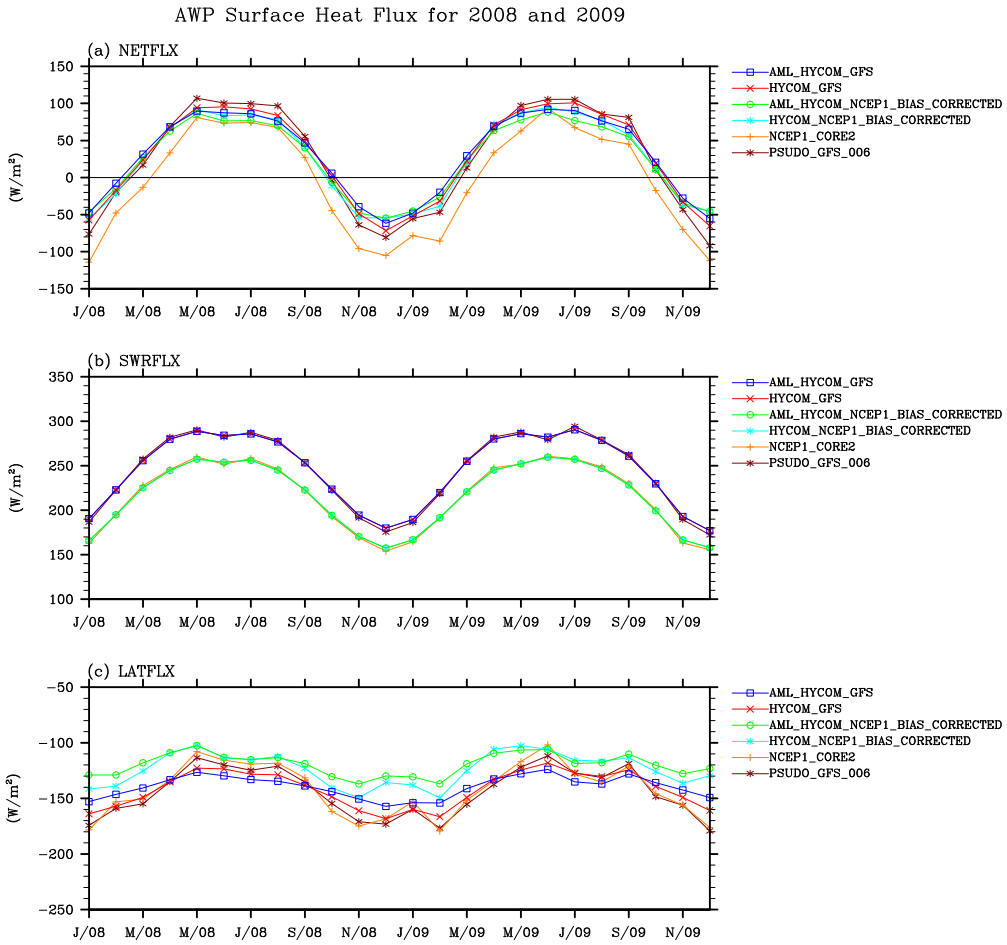


Figure 2-6. (a) Net surface heat flux, (b) shortwave radiative heat flux and (c) latent heat flux in 2008-2009 averaged in the AWP region (100°W-40°W; 5°N-30°N) from two low-resolution HYCOM experiments, two AML-HYCOM experiments, and from two surface flux datasets (i.e., pseudo-GFS, bias-corrected NCEP1). Unit is W/m$^2$.

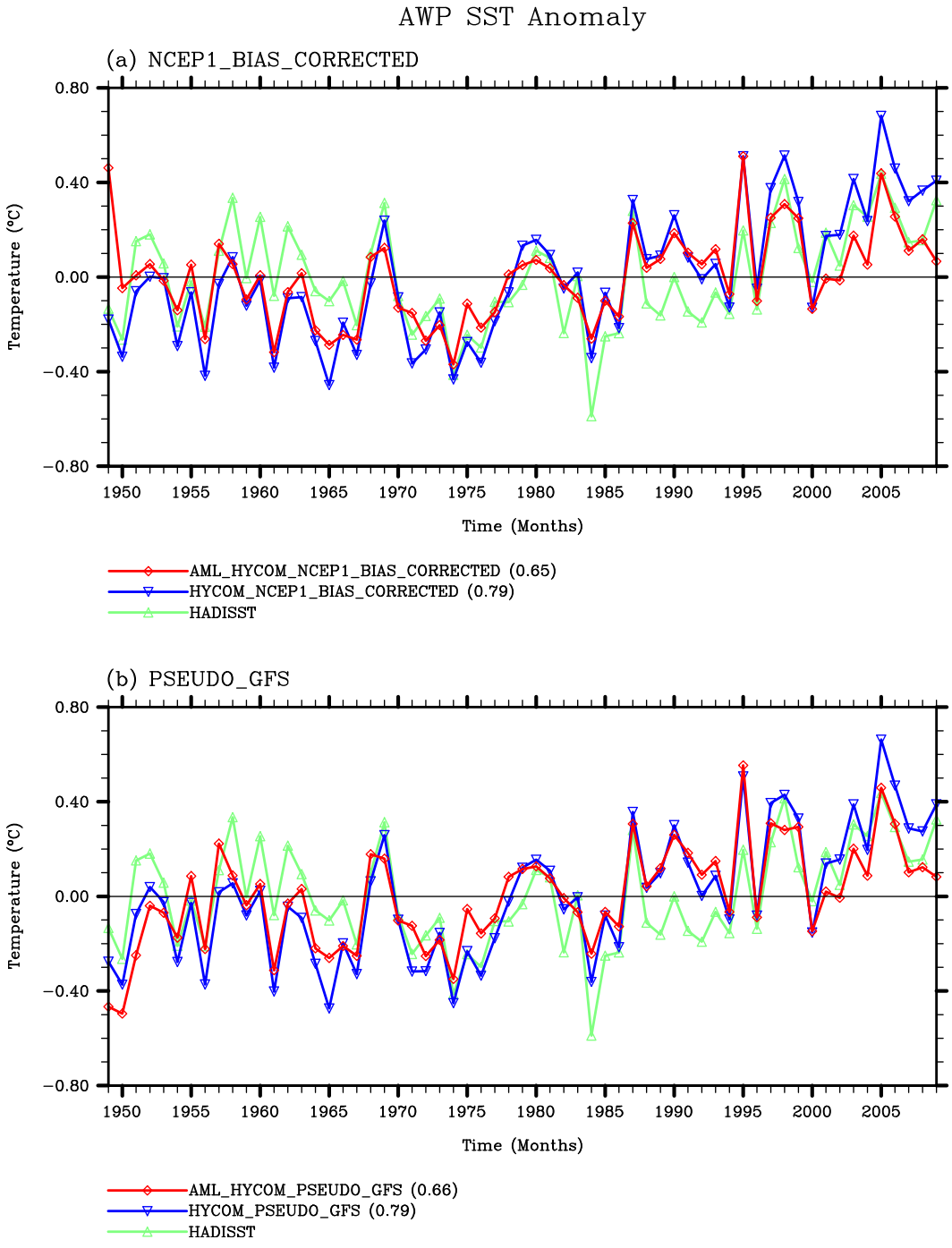


Figure 2-7. Anomalous AWP SST in June-November (JJASON) for the period of 1949-2009 simulated by HYCOM with and without thermal coupling to the AML forced with (a) the bias corrected NCEP1 and (b) pseudo-GFS. Unit is degC.

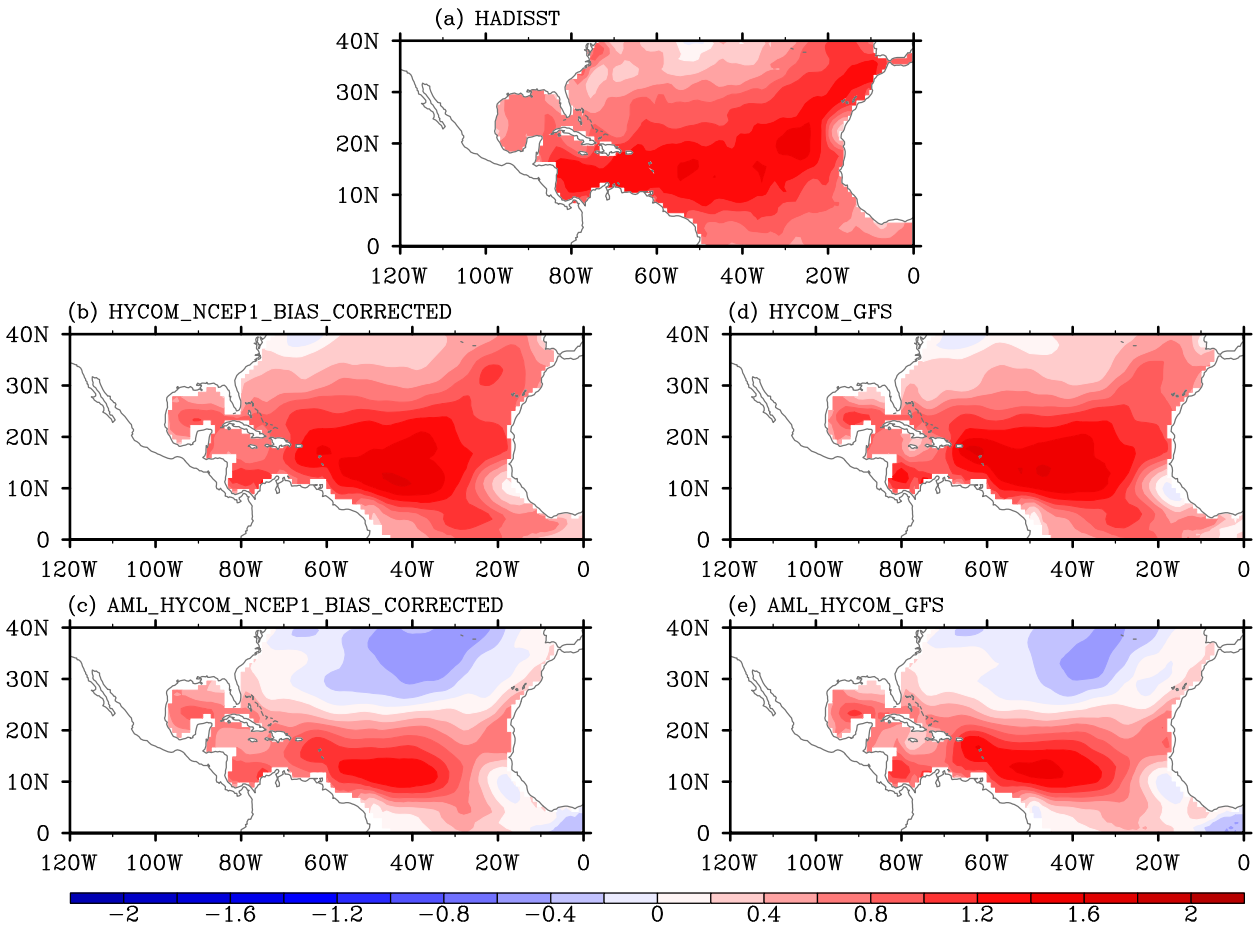


Figure 2-8. Regression coefficients of observed and simulated SST onto the observed AWP SST anomaly in JJASON. Unit is degC/degC.

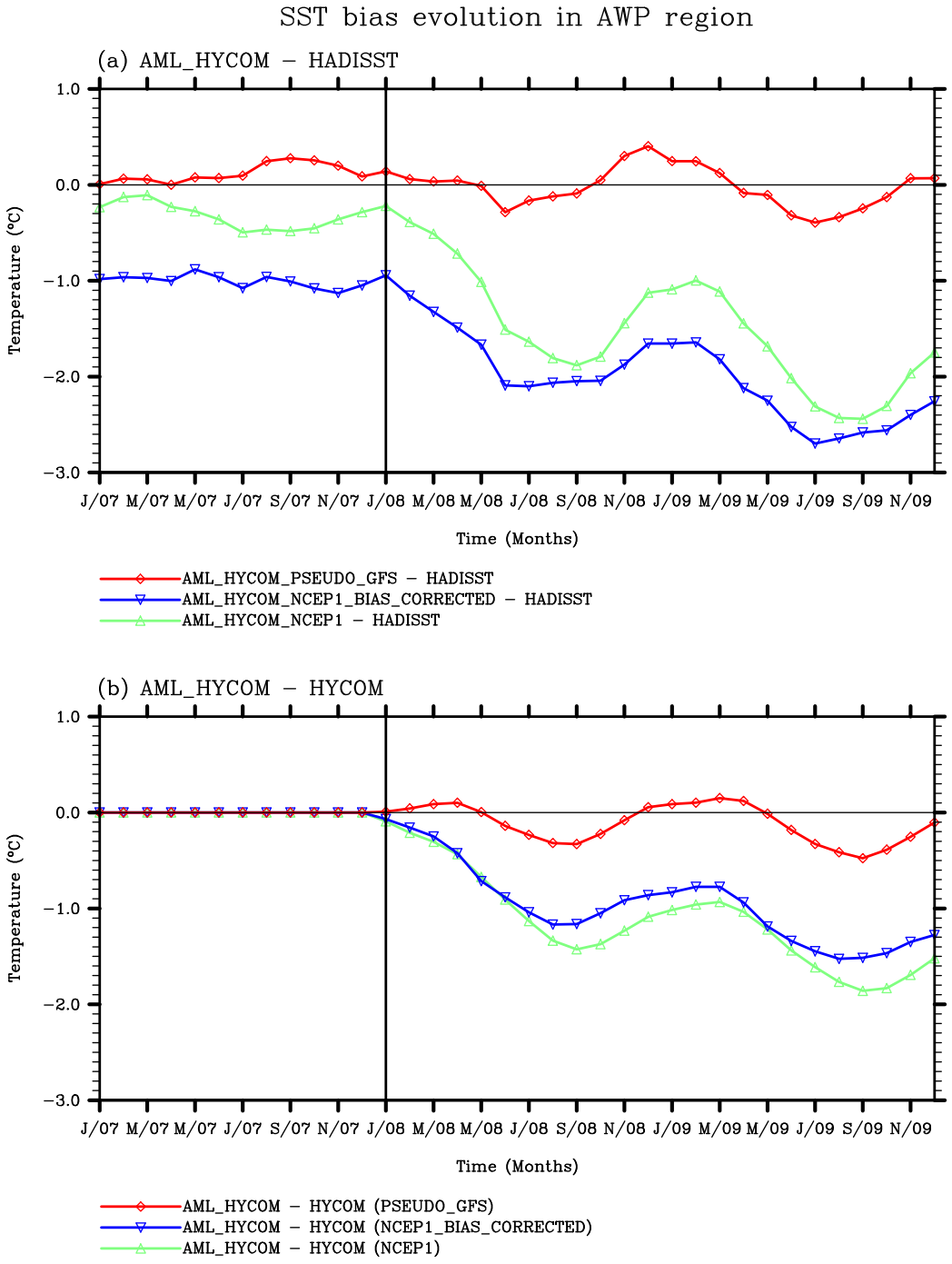


Figure 2-9. Time evolution of simulated AWP SST errors for 2007-2009. The upper panel shows the AWP SST difference between the AML-HYCOM simulation and observation (HADISST). The lower panel shows the AWP SST difference between the AML-HYCOM and forced HYCOM simulations. See text for details. Unit is degC.

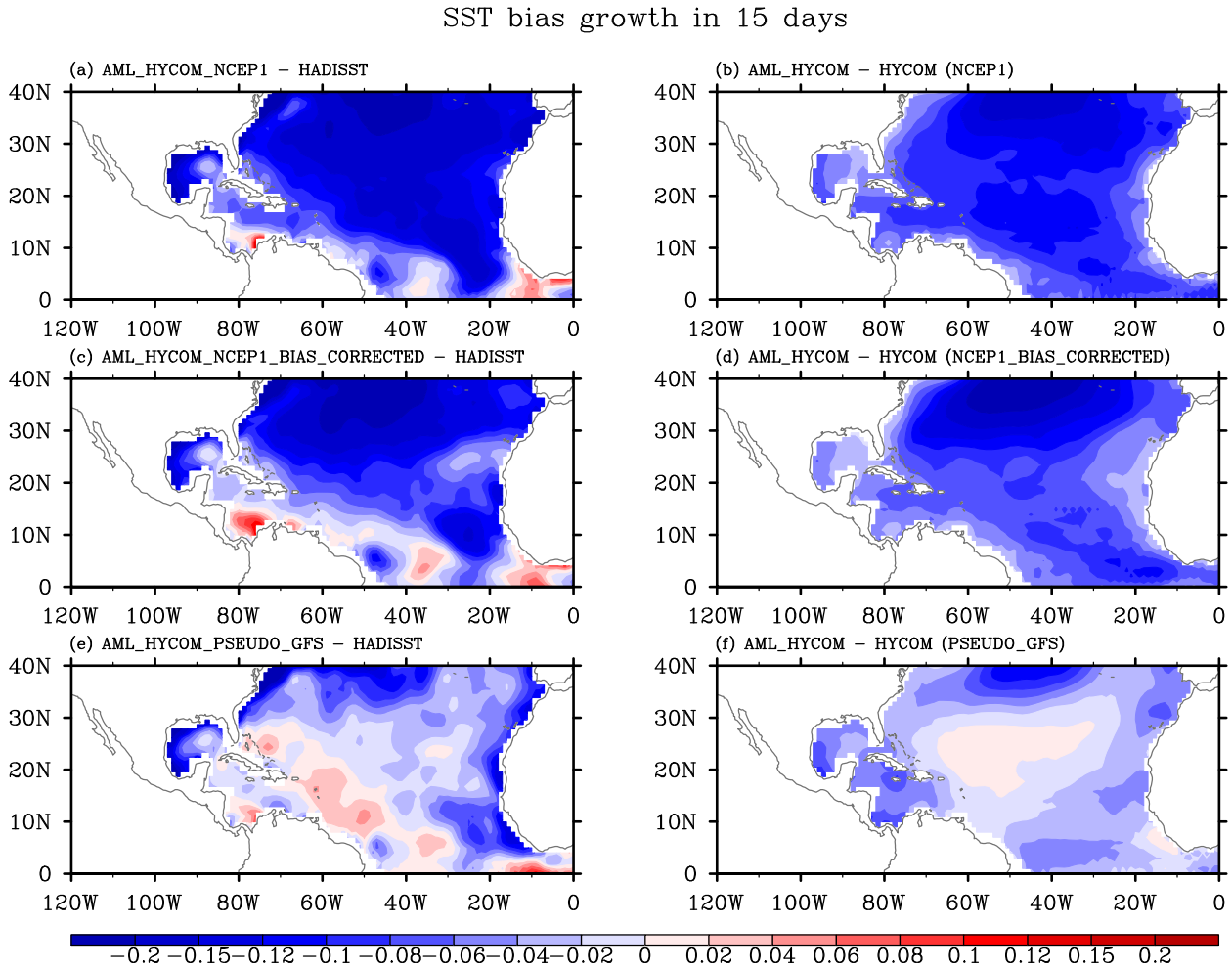


Figure 2-10. Spatial pattern of the expected SST bias growth within 15 days in the thermally coupled HYCOM simulations. Unit is degC.

## 3. AWP forecast in RTOFS

### 3.1. *5-day forecast error in RTOFS during ASO*

Figure 3-1 shows the 5-day forecast error of RTOFS averaged during the each week of August 2010. It is clear that the 5-day forecast error is as large as 2degC and usually negative. In particular, the cold SST error is largest in the deep tropics between equator and 10N. A strong cold SST error is developed during the 4th week over the AWP region of the southern Caribbean Sea and the Gulf of Mexico. It appears that the SST error north of 30N away from the Gulf Stream is largely due to weather forecast error of GFS. Figure 3-2 is same as Figure 3-1 expect during September of 2010. As in Figure 3-1 for August 2010, the 5-day forecast error in this case is large and usually negative. It is still largest in the deep tropics (equator-10N). The southern Caribbean Sea (AWP region) is persistently cold. The eastern tropical North Atlantic SST is also too cold in this case. SST in this region is, however, very difficult to forecast since the mixed layer is very shallow there. In other words, small wind forecast error or ocean initialization error may result in a large SST error. Figure 3-3 is same as Figure 3-1 expect during October of 2010. The regions of large 5-day forecast error are persistently located at the deep tropics, southern Caribbean Sea, and the eastern tropical North Atlantic. However, the spatial structure and strength of the error are changed from the earlier periods. Nevertheless, they evolve rather slowly.

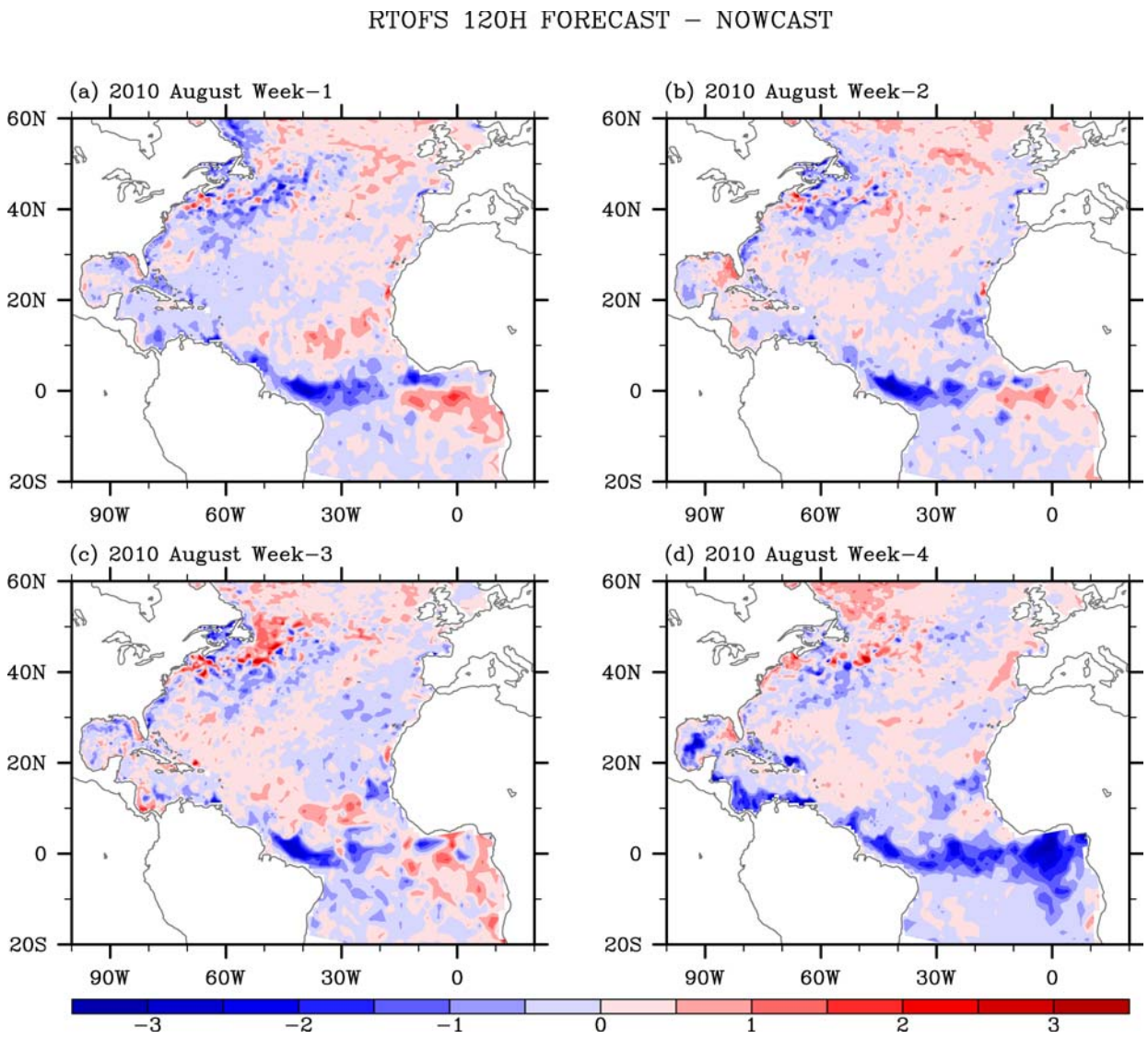


**Figure 3-1**. 5-day forecast error in RTOFS averaged during the each week of August 2010.

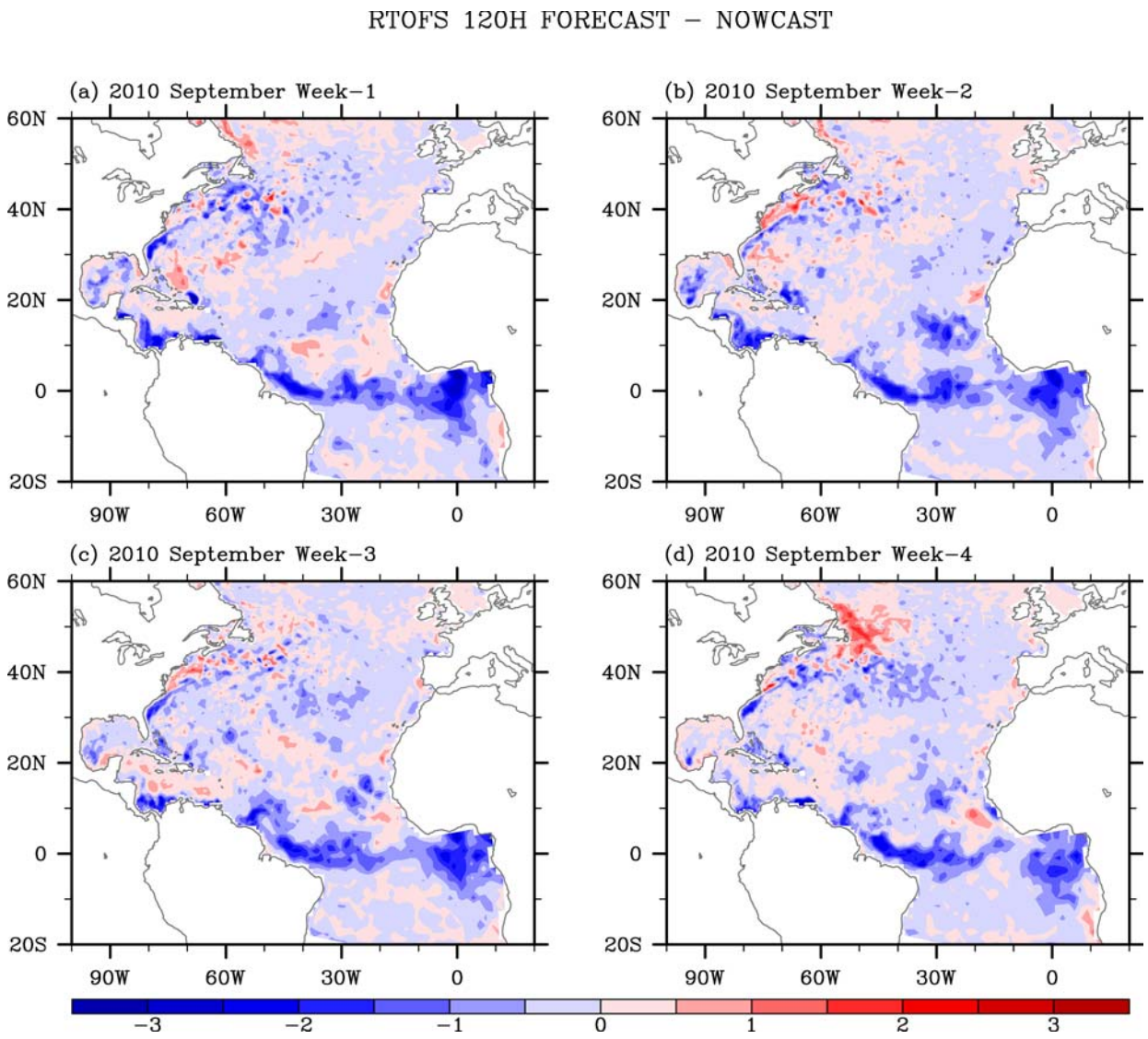


**Figure 3-2**. 5-day forecast error in RTOFS averaged during the each week of September 2010.

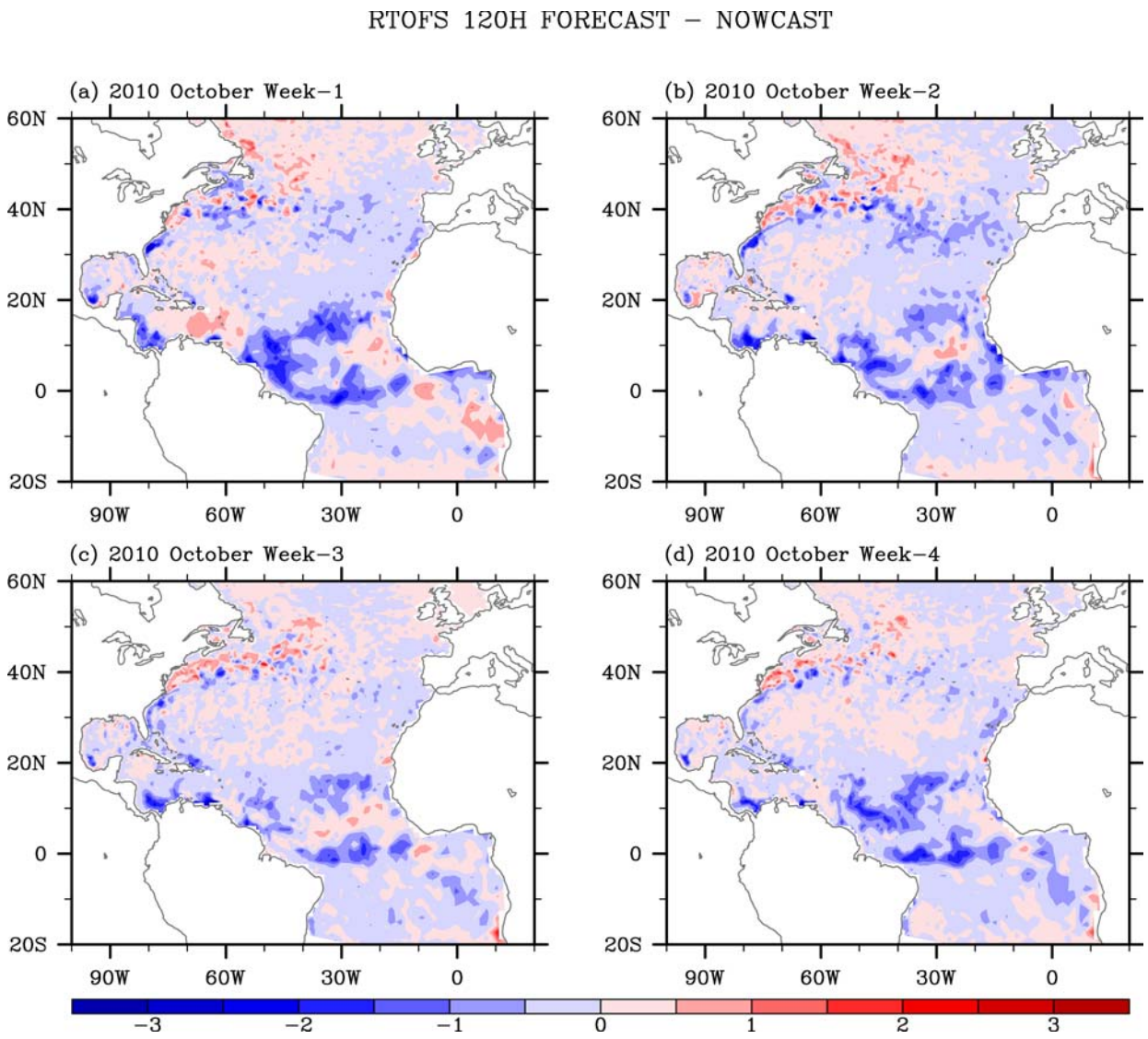


**Figure 3-3**. 5-day forecast error in RTOFS averaged during the each week of October 2010.

Since the 5-day forecast of RTOFS is used, although indirectly, to initialize the HyHWRF every 6 hours, the 5-day forecast error of RTOFS may be potentially introduced to the HyHWRF to negatively affect the hurricane track-and-intensity forecast. However, we found that the SST bias in HYCOM should remains very small within 5-day forecast. Therefore, the 5-day forecast error of RTFS should originate from other sources, that includes

1) Cooper and Haines scheme to project the SSH data to profile data;
2) GFS weather forecast error;
3) Initialization;
4) 2DVAR data assimilation.

3.2. *Application of a simple adaptive bias correction*

Although the spatial structure and strength of the 5-day forecast error change in time, they tend to repeat during a certain period and evolve rather slowly. Therefore, if we assume that the current 5-day forecast error repeats in the next 5-day forecast, we can remove that error in the next 5-day forecast, as shown in the schematic figure (Figure 3-4).

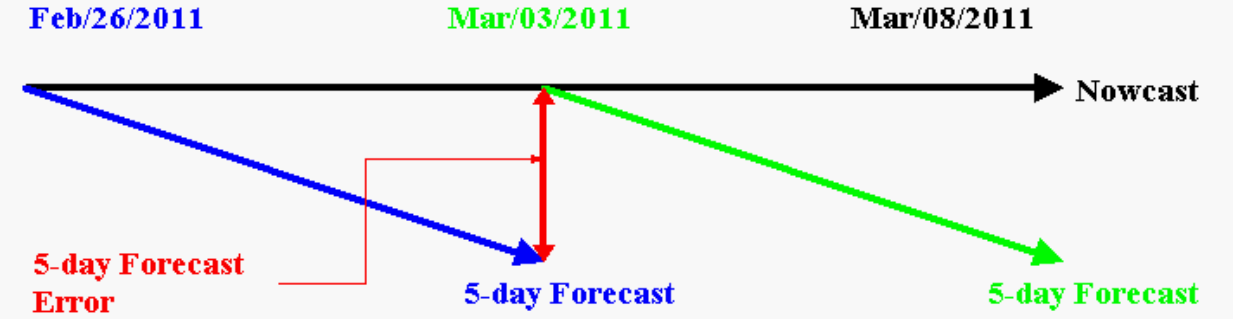


**Figure 3-4**. This schematic figure explains the main idea of the adaptive bias correction scheme used in this study. Assume that today is March/03/2011. Then, we can compute the 5-day forecast error of March/03/2011 (i.e., Nowcast on March/03/2011 - 5-day forecast of March/03/2011). When we make 5-day forecast of March/08/2011, we can remove the 5-day forecast error of March/03/2011.

Figure 3-5 shows the mean and root mean squared error (RMSE) of the 5-day forecast of RTOFS along with the RMSE of the bias-corrected 5-day forecast during August 2010. It is clear that if the adaptive bias correction is applied, the 5-day forecast error is significantly reduced over the deep tropics. However, the RMSE is slightly increased in the high latitude, probably because GFS weather forecast error is amplified there. Figure 3-6 (September 2010) and 3-7 (October 2010) also show that the RMSE can be significantly reduced in the southern Caribbean Sea. Figure 3-8 and 3-9 show that the 5-day forecast RMSE is very large near and entrance of the Caribbean Sea during August and September 2009. The adaptive bias correction significantly reduces this error. As shown in Figure 3-10, during October 2010, the 5-day forecast error is relatively small everywhere. Even in this case, the RMSE is reduced in the southern Caribbean Sea and the deep tropics when the adaptive correction is applied.

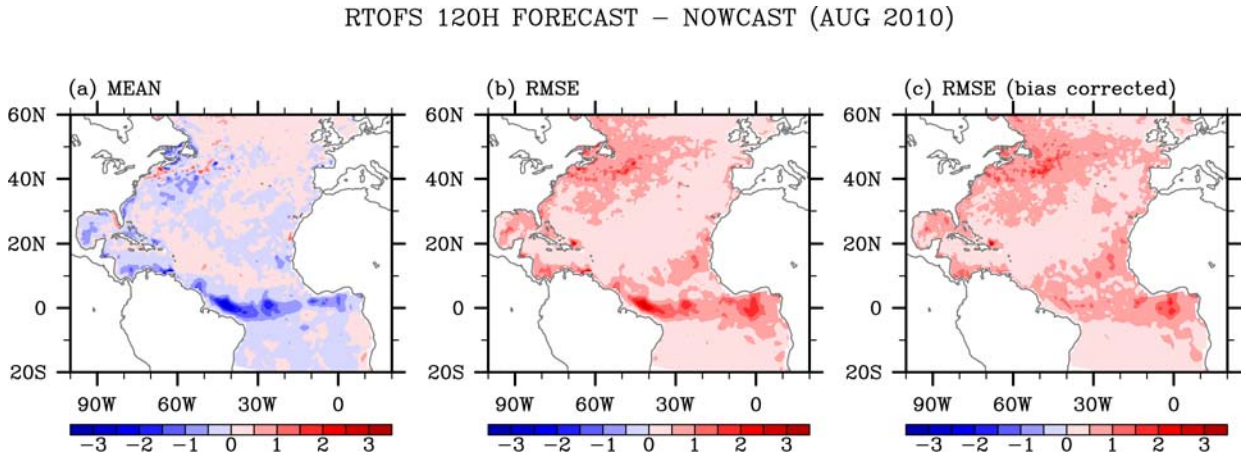


Figure 3-5. (a) Mean and (b) RMSE of the 5-day forecast of RTOFS along with (c) RMSE of the bias-corrected 5-day forecast during August 2010.

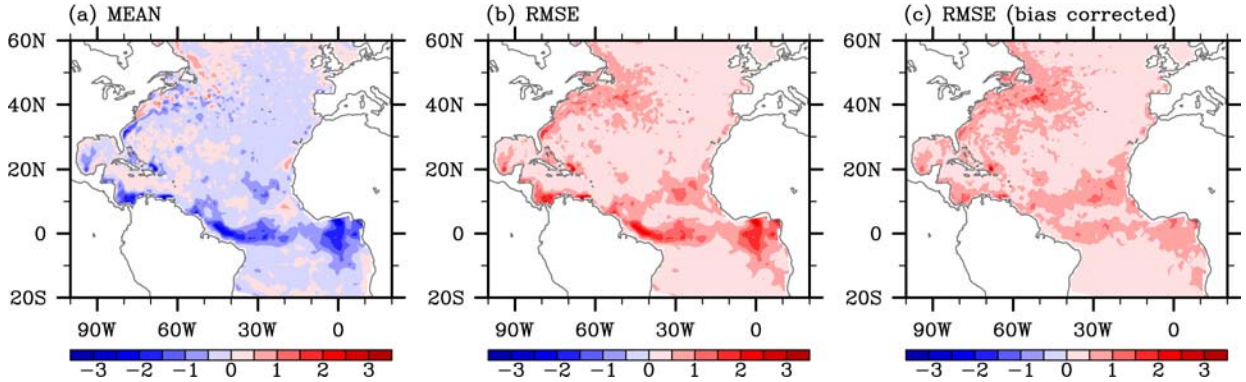


Figure 3-6. (a) Mean and (b) RMSE of the 5-day forecast of RTOFS along with (c) RMSE of the bias-corrected 5-day forecast during September 2010.

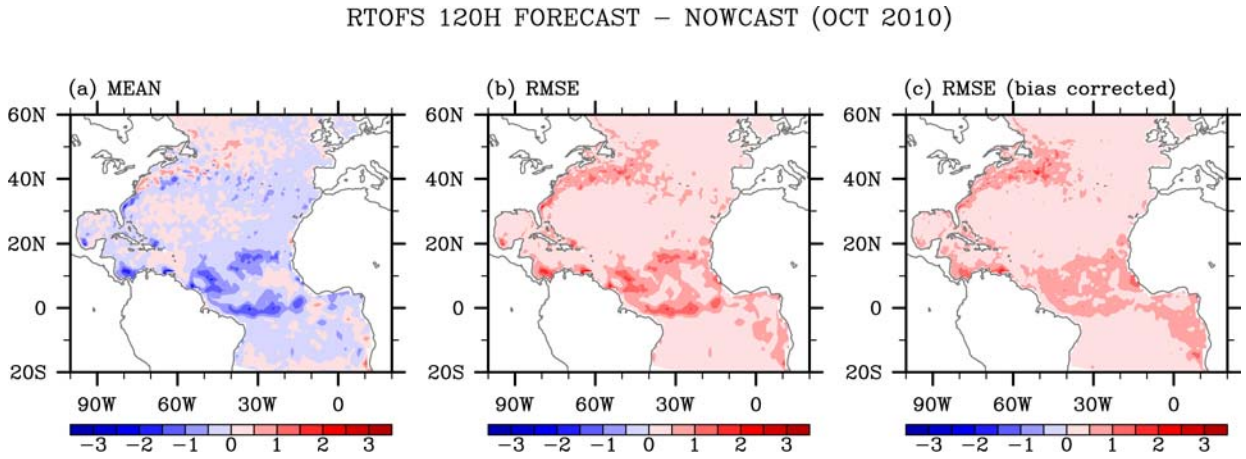


Figure 3-7. (a) Mean and (b) RMSE of the 5-day forecast of RTOFS along with (c) RMSE of the bias-corrected 5-day forecast during October 2010.

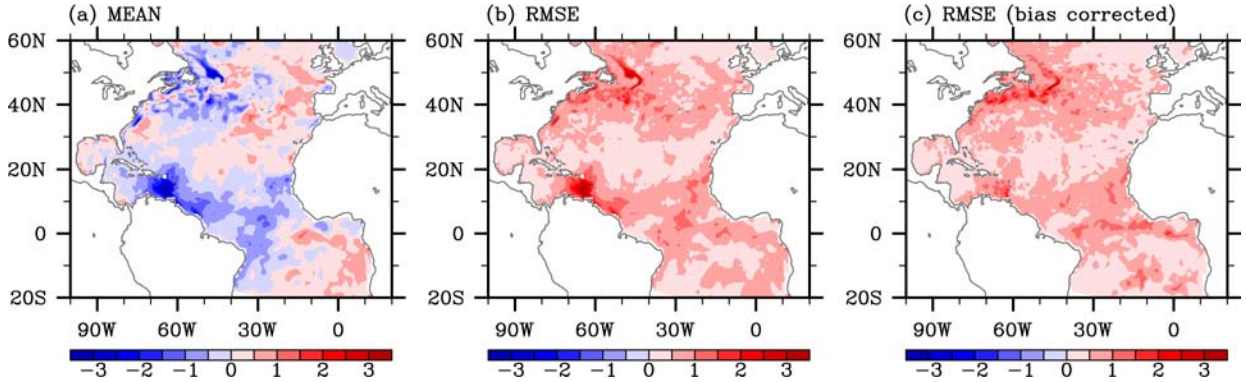


Figure 3-8. (a) Mean and (b) RMSE of the 5-day forecast of RTOFS along with (c) RMSE of the bias-corrected 5-day forecast during August 2009.

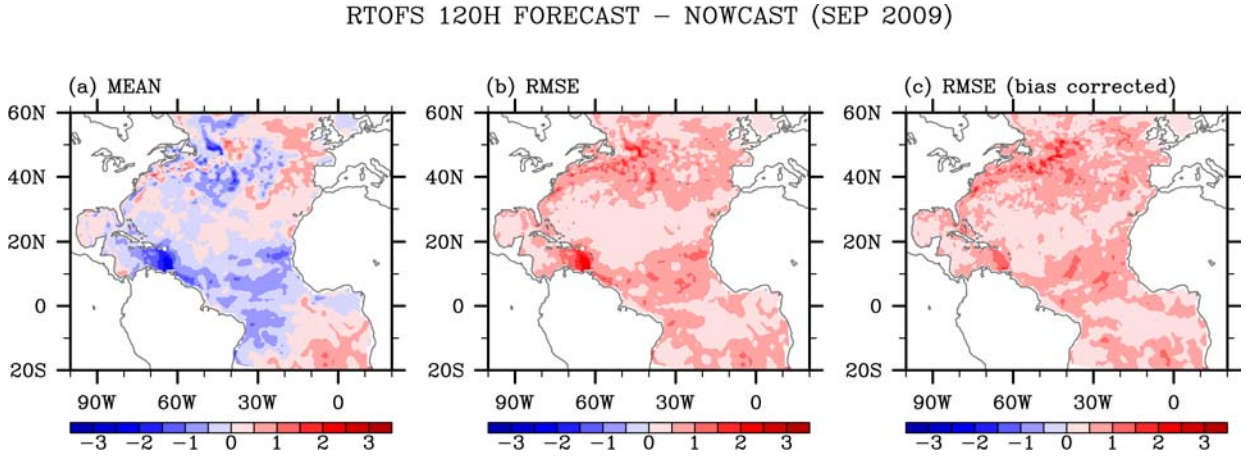


Figure 3-9. (a) Mean and (b) RMSE of the 5-day forecast of RTOFS along with (c) RMSE of the bias-corrected 5-day forecast during September 2009.

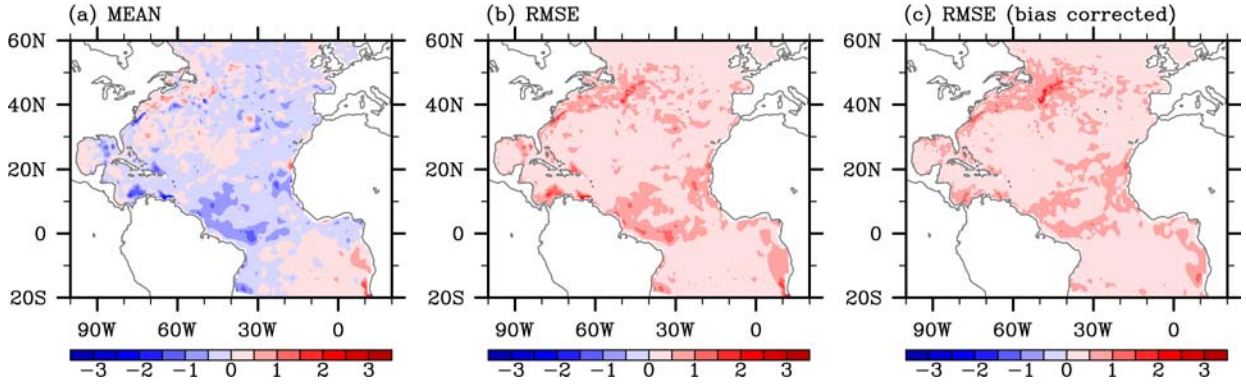


Figure 3-10. (a) Mean and (b) RMSE of the 5-day forecast of RTOFS along with (c) RMSE of the bias-corrected 5-day forecast during October 2009.

For actual implementation of the adaptive bias correction scheme, a corrective surface flux (Qcor) can be computed using the following equation and added to the model's heat equation:

$$\mathrm{Qcor} = \frac{\rho_w c_{pw}}{\mathrm{d}_1} \frac{1}{5} \sum_{\mathrm{i}=1}^{5} \frac{\Delta \mathrm{SST(i)}}{\Delta \mathrm{t(i)}}$$

i means i – day forecast

$\Delta$SST(i) is i - day forecast error

$\Delta$t(i) is the time interval of the i - day forecast

$\mathrm{d}_1$ is the model thikness of the first layer

The adaptive bias correction should not be applied poleward of 30N because GFS weather noise is amplified when the adaptive bias correction scheme is applied there. It is important to point out that the adaptive bias correction scheme does not depend on the details of the model

configuration or data assimilation scheme used. Therefore, if implemented, this scheme will automatically adapt to the future changes in RTOFS.

## 4. Impact of the AWP on U.S. landfalling hurricanes

### 4.1. *Background*

Almost all of the severest hurricane-related loss and damage occur when hurricanes make landfall. Thus, a better understanding of factors controlling hurricane's landfall is both scientifically and socially important. The Atlantic hurricane season officially starts on June 1 and ends on November 30. An average hurricane season, based on the data from 1950-2000 without considering short-lived storms [*Landsea et al*., 2010], has 9.6 named storms and an accumulated cyclone energy (ACE) index of 96.1 (a measure of overall tropical cyclone activity with the unit of $10^4$ $kt^2$) [e.g., *Klotzbach and Gray*, 2006]. Of these 9.6 storms, 5.9 are hurricanes (categories 1-5) and 2.5 are major hurricanes (categories 3-5). The average ratio between U. S. landfalling hurricanes and total hurricanes is about 25%. However, an active hurricane season does not necessarily mean more U.S. landfalling hurricanes because the hurricane track is determined by both the hurricane internal dynamics and large-scale climate variations.

The 2010 Atlantic hurricane season had 19 named storms, 12 hurricanes, 5 major hurricanes and an ACE index of 166.3, all of which indicate that the 2010 season was extremely active. However, for the 2010 hurricane season, not a single hurricane made landfall in the United States. As shown in Figure 4-1a, there were 6 tropical storms and hurricanes that made landfall in Central America, and one tropical storm that made landfall in Florida. But, these were largely short-lived tropical storms that formed in the Caribbean Sea. Excluding those that formed in the Caribbean Sea, Figure 4-1b shows that tropical storms and hurricanes formed in the main development region (MDR) moved northwestward and then recurved northeastward to the subtropical North Atlantic, with the exception of two storms that dissipated near the MDR.

In this paper, we mainly focus on the tropical cyclones (TCs) that formed in the MDR and investigate why and how an active season can occur without a hurricane to make landfall in the United States. The new finding is that a large Atlantic warm pool (AWP) induces barotropic stationary wave patterns that weaken the North Atlantic subtropical high (NASH) and produces the eastward steering flow anomalies along the eastern seaboard of the United States. This AWP-induced steering flow pattern is unfavorable for a hurricane to make landfall in the United States. In addition, the large AWP in 2010 associated with the TC steering flow patterns also explained why no hurricanes made landfall in the U. S. during the 2010 hurricane season. The paper also discusses the impact of other climate phenomena on the hurricane track.

### 4.2. *Data Sets and Model Experiments*

The first data set is the NOAA extended reconstructed SST version 3 [*Smith et al*., 2008], and the second one is the NCEP-NCAR reanalysis [*Kalnay et al*., 1996]. Hurricane data are from HURDAT reanalysis database (http://www.aoml.noaa.gov/hrd/data_sub/re_anal.html). What we use here includes the ACE, all hurricanes, major hurricanes, total named storms, and TC track density. The ACE index is calculated by summing the squares of the estimated maximum sustained wind of every TC, at six-hour intervals. Based on the best-track hurricane data of HURDAT, TC track density is computed by counting the number of TCs passing through each 5°×5° grid box for a given calendar year. Since the hurricane data are relatively reliable after the satellite measurements, here we use the hurricane data from 1970 to 2009. We also use

the hurricane data from 1950 to 2009 and get the similar results (Figs. 3 and S9). The 2010 hurricane data is from NOAA National Hurricane Center (http://www.nhc.noaa.gov/2010atlan.shtml).

The NCAR community atmospheric model version 3.1 (CAM3) is forced by the Hadley Centre SST (HadSST) on a 1°×1° resolution. Based on the HadSST of 1949-2001, we compute monthly SST composites for large AWP (six large AWP years are 1952, 1958, 1969, 1987, 1995, and 1998) and small AWP (seven small AWP years are 1971, 1974, 1975, 1976, 1984, 1986, and 1992). We use these SST composites to perform two sets of ensemble model simulations: large AWP (LAWP) and small AWP (SAWP). In the LAWP run, the twelve-monthly SSTs for the large AWP composites are used in the AWP region for forcing CAM3, while the monthly climatology is specified for the rest of the global ocean. In the set of the SAWP simulation, CAM3 is forced by the small AWP monthly SST composites in the AWP region and climatological SST elsewhere. For the detailed model experiments, see *Wang et al*. [2008a].

4.3. *Role of the AWP in the Hurricane Track*

The influence of the AWP on the TC track operates through at least two ways. The first one is the AWP-related shift of the TC genesis location. The AWP in August-October (ASO) expands toward the east during large AWP years, whereas it contracts during small AWP years (Figs. 2a and b). The eastward shift of warm water and its associated reduction of vertical wind shear result in increased TC activity [*Bell and Chelliah*, 2006; *Kossin and Vimont*, 2007; *Wang et al*., 2008b]. As shown in Figs. 2a and b, more TCs are formed east of 40°W in large AWP years due to the increased SST and atmospheric convective instability there. Figures 4-2c and d show the tracks of TCs that formed in the MDR for large and small AWPs, with blue (red) color representing TCs formed in the east (west) of 40°W. Based on Figs. 2c and d, the ratios of U. S. landfalling TCs (i.e., the number of landfalling TCs divided by the total number of TCs) in the east and west of 40°W are 13.2% and 29.0%, respectively. This indicates that TCs formed further eastward have less opportunity to make landfall in the United States. Therefore, a large AWP shifts the TC genesis location eastward which increases the possibility for a hurricane to move northward without making landfall in the United States.

The result is consistent with the southeastward shift of the genesis location for the strongest Atlantic meridional mode (AMM) years [*Kossin and Vimont*, 2007; *Kossin et al*., 2010]. The AMM is a climate mode of variability intrinsic to the tropical coupled ocean-atmosphere system and involves a positive feedback between surface wind, evaporation and SST. Thus, a strong AMM may be associated with or induce a large AWP, resulting in the eastward shift of the TC genesis location.

The second way is that the AWP induces the changes of atmospheric circulation pattern to influence the TC track. The movement of TCs or the TC track is mainly steered by the surrounding environmental flow in the troposphere and modified by the beta-effect. An integrated flow through a layer of the atmosphere is usually defined as the TC steering flow [e.g., *Dong and Neumann*, 1986]. To examine the influence of the AWP on the TC steering flow, we calculate the steering flow anomalies for large and small AWP years. For large AWP years, Figure 4-3a displays an anomalous cyclonic flow over the eastern U. S. and an anomalous anticyclonic flow over Mexico and the eastern North Pacific. Associated with these patterns are the southeastward flow anomalies in the Gulf of Mexico and the northeastward flow anomalies in the southeast seaboard of the U. S. (Figure 4-3a). The opposite is true for small AWP years (Figure 4-3b). Thus, observational data show that a large (small) AWP is associated with the

steering flow which is unfavorable (favorable) for a hurricane to make landfall in the United States. Additionally, the steering flow anomalies in neutral AWP years are very small in comparison with large/small AWP years (not shown), indicating that AWP variability plays a key role for the TC steering flow change.

The relationship between the AWP and TC tracks is further investigated by using the TC track density data from 1970 to 2009. The climatological mean of TC track density is shown in Figure 4-3c. Consistent with that by *Xie et al*. [2005], the center of maximum TC density is located in the western subtropical North Atlantic, reflecting that most of TCs form in the tropical North Atlantic and move northwestward. The impact of the AWP on the TC track is examined by regressing TC track density onto the AWP index (Figure 4-3d). The regression is positive in the entire North Atlantic, reflecting that a large (small) AWP increases (decreases) Atlantic hurricane activity overall [*Wang et al*., 2006]. The regressed map also shows two maxima: one is in the Intra-Americas Sea (IAS), i.e., the Gulf of Mexico and the Caribbean Sea, and the other is located in the subtropical central North Atlantic. The maximum regression in the IAS is due to TCs that form in the IAS typically during the early and late season as in the 2010 season (Figure 4-1). To confirm the result, we exclude all TCs that form in the IAS from the hurricane data and recalculate the regression. As shown in Figure 4-3e, the maximum regression in the IAS almost disappears. The maximum regression in the subtropical central North Atlantic is oriented in a nearly south-to-north direction far away from the U. S. eastern seaboard. This indicates that hurricanes tend to move northward to the subtropical North Atlantic Ocean instead of making landfall in the U. S. during large AWP years. The distributions of TC track density in large and small AWP years also support the results reported here (Figs. S2 and S3).

We next use CAM3 to show that the AWP affects the TC track via the AWP-induced steering flow change. In the tropical North Atlantic, TCs usually move toward the west with a slight poleward component due to an axis of high pressure called the NASH that extends east-west poleward of TCs. On the equatorward side of the NASH, the easterly trade winds prevail. However, if the NASH is weak and/or shifts northeastward, TCs may turn poleward and then recurve toward the east [e.g., *Liu and Fearn*, 2000; *Elsner et al*., 2000]. On the poleward side of the NASH, the westerly winds prevail thus steering TCs back to the east. Hence, both the position and strength of the NASH can determine and change the movement of TCs.

The CAM3 simulated NASHs from the ensemble LAWP and SAWP model runs are shown in Figure 4-4. A comparison of Figs. 4a and b shows that the sea level pressure (SLP) associated with the NASH is significantly decreased (increased) in response to a large (small) AWP. The contour of 1021-hPa for the LAWP run stays in the eastern subtropical North Atlantic, whereas its counterpart for the SAWP run extends westward to the east coast of the United States. Therefore, AWP variability affects both the strength and position of the NASH.

The steering flow patterns associated with the LAWP and SAWP model runs show an anomalous anticyclonic flow centered over the southeastern U. S. and an anomalous cyclonic flow immediately northeastward (Figure 4-4c). The simulated steering flow patterns are consistent with observations although the centers of these steering flow patterns are located slightly northeastward in comparison with the observational results of Figure 4-3. As demonstrated by using a simple two-level atmospheric model [*Lee et al*., 2009], these patterns are the AWP-induced barotropic stationary waves in the boreal/fall summer. These AWP-forced stationary waves produce the eastward flow anomalies along the eastern seaboard of the U. S. that prevent hurricanes from making landfall in the United States. As schematically drawn in Figs. 4a and b, the LAWP-induced northeastward retreat of the NASH will allow a more

frequent northeastward recurvature of hurricanes, whereas the SAWP-induced NASH distribution creates a more favorable condition for hurricanes to make landfall in the United States. In other words, a large AWP does not allow the NASH to extend far west, meaning that hurricanes likely would be steered around NASH's edge to the northeast instead of making landfall in the United States.

4.4. *Impact of Other Climate Factors and the 2010 Hurricane Season*

It is well-known that ENSO can remotely influence Atlantic hurricane activity: a La Niña (El Niño) event in the tropical Pacific increases (decreases) the frequency of Atlantic hurricanes [e.g., *Bell and Chelliah*, 2006]. ENSO's impact on the hurricane track is shown by regressing TC track density onto the Nino3 index (Figure 4-3f). The significant negative regression is located near the IAS, suggesting that cold (warm) SST anomalies in the tropical Pacific increase (decrease) TC density in the IAS. In other words, a La Niña (El Niño) event in the Pacific tends to enhance (suppress) the possibility for a hurricane to make landfall in Central America, Caribbean Islands, and the southeastern United States.

Now, with the relationships among the AWP, ENSO, NASH and hurricane track from historical data and model experiments, it is quite straightforward to explain why the 2010 hurricane season was so active, but without a landfalling hurricane in the United States. The AWP during ASO of 2010 was extremely large, being about 2.2 times larger than its climatological mean (Figure 4-5a). 2010 was also a La Niña year: cold SST anomalies covered the equatorial central and eastern Pacific during the 2010 hurricane season. A combination of the local effect of the large AWP and remote influence of the La Niña condition in the Pacific resulted in an active 2010 season. However, the large AWP in 2010 weakened the NASH and pushed the NASH northeastward (Figs. 5b and d). The negative SLP anomalies in the southwestern tropical North Atlantic indicated a northeastward retreat of the NASH. As shown and discussed earlier, the weakening and the northeastward shift of the NASH tend to make a hurricane move northward and northeastward. Therefore, although climate phenomena in 2010 tended to increase the number of Atlantic hurricanes, the large AWP in 2010 weakened the NASH and prevented the NASH from extending far west, resulting in hurricanes being steered around NASH's edge to the northeast instead of making landfall in the United States. The steering flow anomalies in 2010 showed a cyclonic flow in the western North Atlantic and an anticyclonic flow in the southeastern U. S. (Figure 4-5c). The cyclonic and anticyclonic steering flow patterns in 2010 were similar to the observed ones during the past decades (Figs. 3a and b) and the modeling result (Figure 4-4c). It is clear that the steering flow anomalies in 2010 were favorable for TCs to move northwestward and then recurve northeastward.

Figures 4-3f clearly show that a La Niña event tends to increase the possibility of landfall in the southeastern U. S. and potentially decrease recurving hurricanes. This suggests that the 2010 La Niña event in the tropical Pacific should have favored Atlantic hurricanes to make a landfall, which is not the case in the 2010 hurricane season. Therefore, it can be concluded that the influence of the La Niña event in 2010 may have been offset by an extremely large AWP which displayed the NASH to the northeast of its climatological location.

Other climate phenomena, which may also contribute to Atlantic hurricane activity, include the North Atlantic oscillation (NAO) [e.g., *Elsner et al*., 2000; *Kossin et al*., 2010] and the Atlantic multidecadal oscillation (AMO) [e.g., *Goldenberg et al*., 2001]. Tthe NAO index is extremely low in the year of 2010 relative to its climatology (not shown). Since the NAO index represents variations of the Icelandic low and the NASH, the low NAO index in 2010 may be

associated with a weakening of the NASH. This seems to suggest that the observed weakening and northeastward movement of the NASH during 2010 in Figure 4-5 may also include the effect of the NAO. However, the relationship of the NAO with TC track density is not significant except in the extratropics (not shown). Regarding AMO's impact, it has been shown that the AWP serves as a link between the AMO and Atlantic hurricane activity [*Wang et al*., 2008b]. Therefore, the influence of the AMO on hurricanes may operate through the mechanism of the AWP-induced atmospheric changes. This is supported by the similar regressed TC track density patterns for the AMO (Figs. S7b and S7c) and the AWP (Figs. 3d and e).

4.5. *Summary and Discussion*

The paper shows that the AWP affects the Atlantic TC track, in addition to the increase in the number of TCs. A large AWP shifts the TC genesis location eastward, so it increases the chance for a TC to move northward without making landfall in the United States. A large AWP also weakens the NASH and thus induces the northward and northeastward steering flow anomalies, which steer hurricanes away from the United States. Other climate phenomena such as ENSO and the NAO cannot explain the lack of landfalling hurricanes in 2010. An implication of this study is that a better prediction of climate variability can help improve the U. S. landfalling hurricane outlook.

In this paper, we use the data from 1970-2009 to identify large AWP years by the top quartiles of the AWP index (1987, 1998, 2001, 2003, 2004, 2005, 2006, 2007, 2008, and 2009) and small AWP years by the bottom quartiles of the AWP index (1971, 1974, 1975, 1976, 1982, 1984, 1985, 1986, 1992, and 1994). These ten large and small AWP years are respectively associated with 31 and 13 hurricanes that form in the MDR, of which 7 and 5 hurricanes make landfall in the United States. This indicates that (1) the large AWP increases the number of hurricanes formed in the MDR, and (2) but the large AWP decreases the ratio of U. S. landfalling hurricanes by about 40%.

The factors controlling the TC track are complicated, determined by the TC internal dynamics and large-scale climate as well as synoptic weather patterns. As an example, 2005 was a busy season and also had more landfalling hurricanes (five of fifteen hurricanes in 2005 made landfall in the U. S.). The AWP in 2005 was large although it was smaller than that in 2010 (not shown). The SLP anomalies are negative in the AWP region, but near neutral over the U. S. (not shown). The lack of SLP response over the U. S. may be due to different teleconnections induced by different AWP heating patterns or different latitudinal positions of the subtropical jet [*Lee et al*., 2009]. Associated with the SLP distributions are the steering flow anomalies showing the westward and northwestward flows in the tropical North Atlantic and the AWP region (not shown), which were favorable for hurricanes to make landfall. Nevertheless, of the four hurricanes formed in the MDR during 2005, one made landfall in Central America and the other three moved northward without landfalling in the United States. The 2005 hurricane season is not inconsistent with the results presented in this paper.

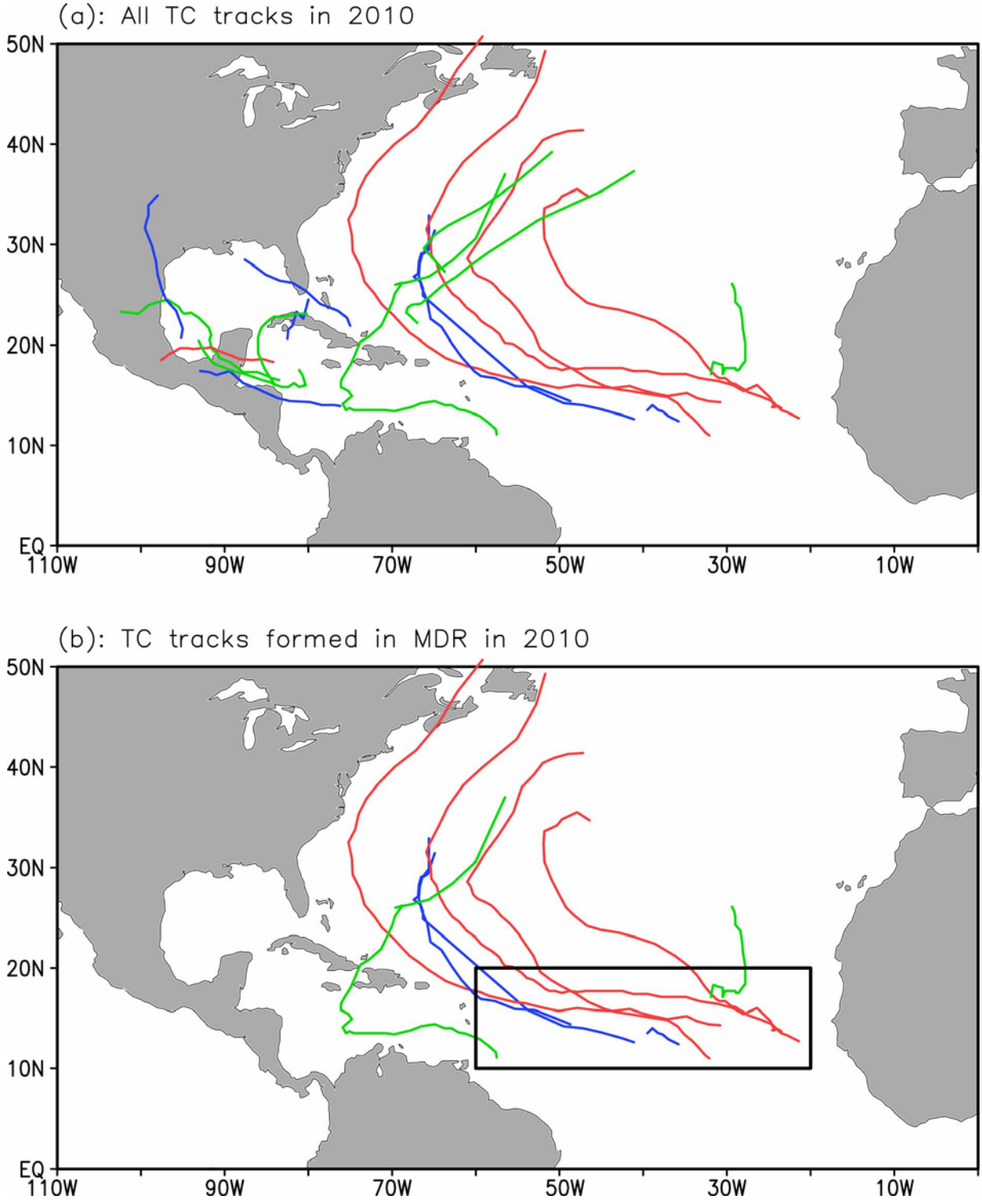


**Figure 4-1.** TC tracks in the 2010 Atlantic hurricane season. Shown are (a) all TCs in the 2010 season and (b) TCs that formed in the MDR indicated by the box (10°N-20°N, 60°W-20°W). TCs that reached major hurricane (Category 3-5) intensity are in red color and TCs that reached Category 1-2 hurricane intensity are in green color.

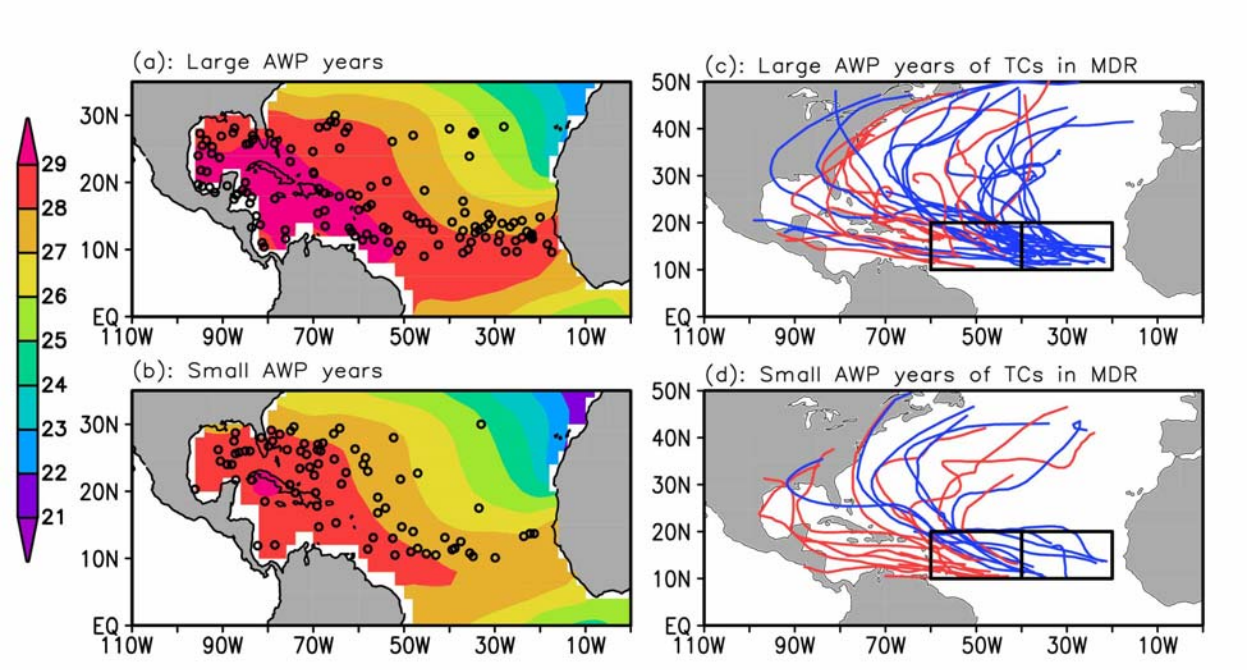


**Figure 4-2.** The TC genesis location, TC track and AWP variability. Shown are the TC genesis location (dots) and SST (shading) for (a) large and (b) small AWP years and the tracks of TCs that formed in the MDR for (c) large and (d) small AWPs. Based on the data from 1970 to 2009, the top and bottom quartiles of the ASO AWP index are identified as large and small AWP years, respectively. The composites of SST for large and small AWP years are then computed. The dots represent the location of all TCs formed southward of 30°N in large (126 TCs) and small (79 TCs) AWP years. In (c) and (d), 38 (31) TCs are formed in the east (west) of 40°W with 5 (9) TCs making landfall in the United States.

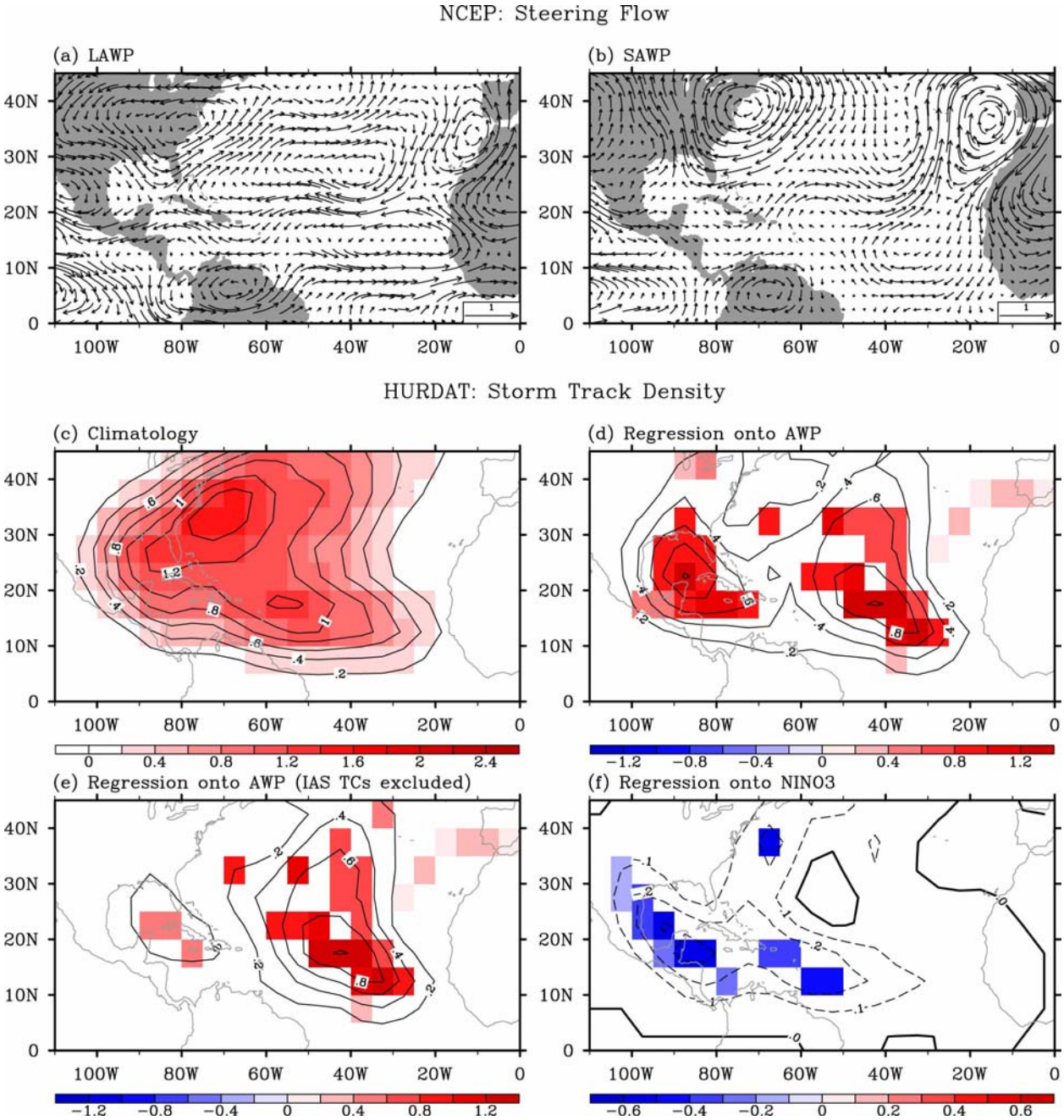


**Figure 4-3.** The TC steering flow and TC track density, and their relationship with AWP and ENSO variability during ASO. Shown are the TC steering flow anomalies ($\times 10^3$ hPa m/s) for (a) large and (b) small AWP years, (c) the climatological mean of TC track density (the number), (d) the regression coefficient (the number per 100%) of TC track density onto AWP index, (e) the regression coefficient (the number per 100%) of TC track density onto AWP index with IAS TCs excluded, and (f) the regression coefficient (the number per °C) of TC track density onto Nino3 index. In (d)-(f), the regression coefficients higher than the 95% significant level are shaded. The AWP index is calculated as the anomalies of the area of SST warmer than 28.5°C divided by the climatological ASO AWP area. Based on the data from 1970 to 2009, the top and bottom quartiles of the AWP index are identified as large and small AWP years, respectively. The

steering flow anomalies are computed by compositing the vertically-averaged wind anomalies from 850 hPa to 200 hPa for large and small AWP years.

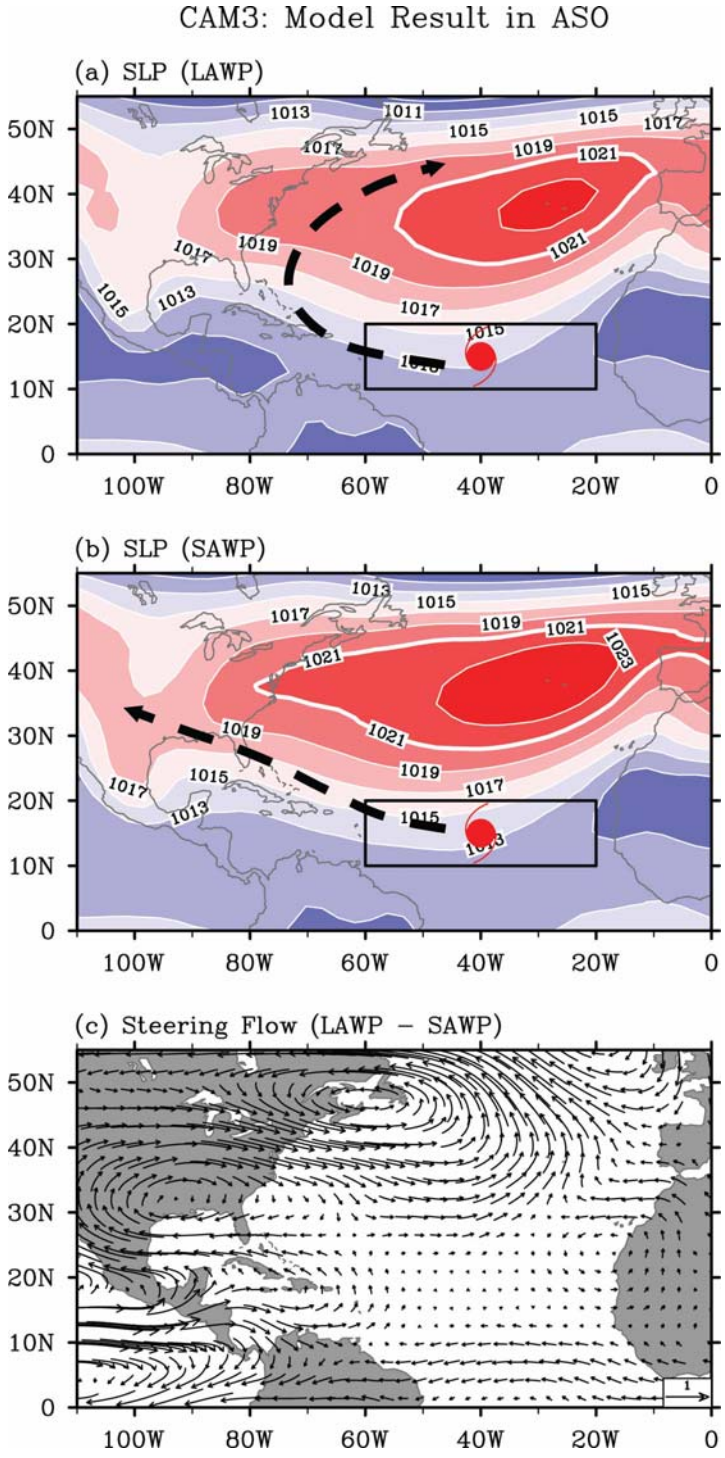


**Figure 4-4.** The simulated effect of the AWP on the NASH from the CAM3 runs during ASO. Shown are the SLPs for the (a) large AWP (LAWP) run, (b) small AWP (SAWP) run and (c) steering flow difference between LAWP and SAWP runs. The steering flow ($\times 10^3$ hPa m/s) is calculated as the vertically-averaged wind from 850 hPa to 200 hPa. The dashed arrows are schematically drawn, illustrating the hurricane track if a hurricane forms in the MDR.

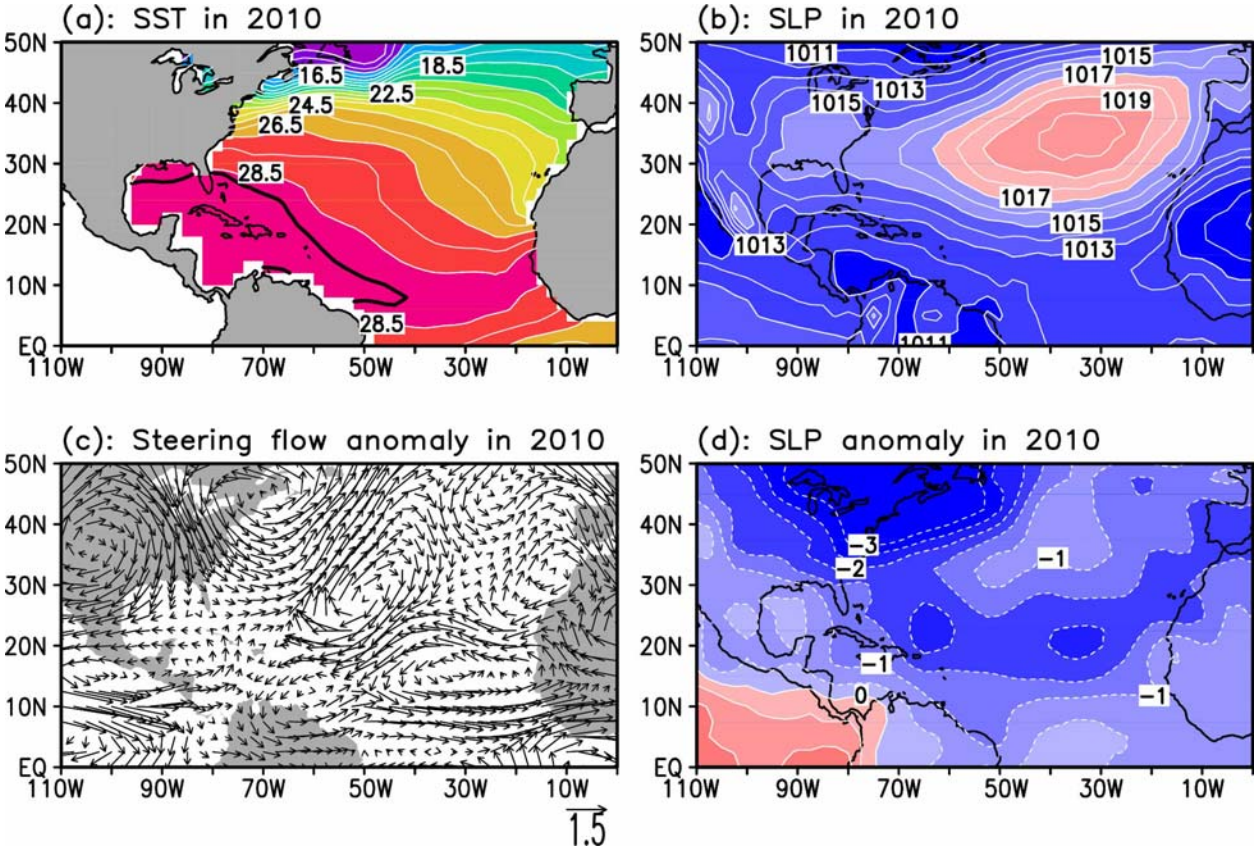


**Figure 4-5.** The AWP, NASH and steering flow during ASO of 2010. Shown are (a) the SST, (b) the SLP, (c) the steering flow anomalies ($\times 10^3$ hPa m/s), and (d) the SLP in ASO of 2010 minus climatological ASO SLP. The AWP is defined by SST warmer than 28.5°C. The dark contour in (a) represents the climatological ASO AWP.

## 5. Publications

Wang, C., H. Liu, S.-K. Lee, and R. Atlas, 2011. Impact of the Atlantic warm pool on United States landfalling hurricanes, *Geophys. Res. Lett*., In-Press.

Lee, S.-K., D. B. Enfield and C. Wang, 2011. Future impact of differential inter-basin ocean warming on Atlantic hurricanes. , *J. Clim.,* **24**, 1264-1275.

Lee, S.-K., C. Wang and D. B. Enfield, 2010. On the impact of central Pacific warming events on Atlantic tropical storm activity. *Geophys. Res. Lett*, 37, L17702, doi:10.1029/2010GL044459.

Wang C. and S.-K. Lee, 2010. Is hurricane activity in one basin tied to another? *EOS*, 91, 93-94, doi:10.1029/2009ES002729.

## 6. References

Bell, G. D., and M. Chelliah (2006), Leading tropical modes associated with interannual and multidecadal fluctuations in North Atlantic hurricane activity, *J. Clim., 19*, 590-612.

Dong, K., and C. J. Neumann (1986), The relationship between tropical cyclone motion and the environmental geostrophic flows, *Mon. Weather Rev., 114*, 115-122.

Elsner, J. B., K.-B. Liu, and B. Kocher (2000), Spatial variations in major U.S. hurricane activity: Statistics and a physical mechanism, *J. Clim., 13*, 2293-2305.

Enfield, D.B., S.-K. Lee, 2005: The Heat Balance of the Western Hemisphere Warm Pool. *J. Climate*, **18** (14), 2662-2681.

Goldenberg, S. B., C. Landsea, A. M. Mestas-Nunez, and W. M. Gray (2001), The recent increase in Atlantic hurricane activity, *Science, 293*, 474-479.

Kalnay, E., and Co-authors (1996), The NCEP/NCAR 40-year reanalysis project, *Bull. Am. Meteorol. Soc*., *77*, 437-471.

Klotzbach, P. J., and W. M. Gray (2006), Causes of the unusually destructive 2004 Atlantic basin hurricane season, *Bull. Amer. Meteor. Soc*., *87*, 1325-1333.

Kossin, J. P., and D. J. Vimont (2007), A more general framework for understanding Atlantic hurricane variability and trends, *Bull. Amer. Meteor. Soc*., *88*, 1767-1781.

Kossin, J. P., S. J. Camargo, and M. Sitkowski (2010), Climate modulation of North Atlantic hurricane tracks, *J. Clim., 23*, 3057-3076.

Landsea, C. W., G. A. Vecchi, L. Bengtsson, and T. R. Knutson (2010), Impact of duration thresholds on Atlantic tropical cyclone counts, *J. Clim. 23*, 2508-2519.

Large, W.G. and S.G. Yeager, 2008: The Global Climatology of an Interannually Varying Air-Sea Flux Data Set. *Clim. Dyn.*, doi:10.1007/s00382-008-0441-3.

Lee, S.-K., D.B. Enfield, C. Wang, 2005: Ocean General Circulation Model Sensitivity Experiments on the Annual Cycle of Western Hemisphere Warm Pool. *J. Geophys. Res*., **110**, doi:10.1029/2004JC002640.

Lee, S.-K., D.B. Enfield, C. Wang, 2007: What drives the seasonal onset and decay of the Western Hemisphere warm pool? *J. Climate*, **20**, 2133-2146.

Lee, S.-K., C. Wang, and B. E. Mapes (2009), A simple atmospheric model of the local and teleconnection responses to tropical heating anomalies, *J. Clim*., 22, 272-284.

Liu, K.-B., and M. L. Fearn (2000), Reconstruction of prehistoric landfall frequencies of catastrophic hurricanes in Northwestern Florida from Lake sediment records, *Quat. Res*., *54*, 238-245.

Seager, R., M.B. Blumenthal, and Y. Kushnir, 1995: An Advective Atmospheric Mixed Layer Model for Ocean Modeling Purposes: Global Simulation of Surface Heat Fluxes. *J. Climate*, **8**, 1951–1964.

Smith, T. M., R. W. Reynolds, T. C. Peterson, and J. Lawrimore (2008), Improvements to NOAA's Historical Merged Land-Ocean Surface Temperature Analysis (1880-2006), *J. Clim*., *21*, 2283-2296.

Wang, C., D. B. Enfield, S.-K. Lee, and C. W. Landsea (2006), Influences of the Atlantic warm pool on Western Hemisphere summer rainfall and Atlantic hurricanes, *J. Clim., 19*, 3011-3028.

Wang, C., S.-K. Lee, and D. B. Enfield (2008a), Climate response to anomalously large and small Atlantic warm pools during the summer, *J. Clim., 21*, 2437-2450.

Wang, C., S.-K. Lee, and D. B. Enfield (2008b), Atlantic warm pool acting as a link between Atlantic multidecadal oscillation and Atlantic tropical cyclone activity, *Geochem. Geophys. Geosyst*., *9*, Q05V03, doi:10.1029/2007GC001809.

Xie, L., et al. (2005), Climatology and interannual variability of North Atlantic hurricane tracks, *J. Clim., 18*, 5370-5381.